

8. IDENTIFICATION OF MIXED-LAYERED CLAY MINERALS	261
Méring's Principles and Mixed-Layered Nomenclature	263
The Q Rule, a Broadening Descriptor	266
Mixed-Layered Clay Minerals	270
Illite/Smectite	270
Chlorite/Smectite and Chlorite/Vermiculite	276
Kaolinite/Smectite	284
Serpentine/Chlorite	289
Mica/Vermiculite	292
Summary	296
References	296

Chapter 8

Identification of Mixed-Layered Clay Minerals

X-ray diffraction patterns of mixed-layered (or interlayered or interstratified) clay minerals pose some of the most difficult problems of interpretation, particularly if, as is often the case, the mixed-layered species are present in physical mixtures that include the simple clay types. Multiple analyses are the rule. They use all the available strategies such as heat treatments and solvation with water and ethylene glycol (EG). To identify mixed-layered species successfully, you need to consider the entire diffraction pattern, because the breadth and symmetry of each diffraction peak may be diagnostic, together with the peak position and intensity. This chapter contains representative examples of diffraction patterns, but more extensive coverage of each of the mineral types is discussed in Reynolds (1980). The theory upon which calculated diffraction patterns are based was developed by MacEwan (1958), augmented by Reynolds (1967), applied by Reynolds and Hower (1970), and described in detail by Reynolds (1980). All calculated diffractograms shown here have been calculated with the computer program NEWMOD[©] (Reynolds, 1985, see the Appendix). They are all calculated based on CuK α radiation, unless noted otherwise. No attempts have been made to portray correct absolute intensities or correct relative intensities between patterns. The vertical scales have been selected either to scale the strongest peaks to 100% or to emphasize the details of the weaker reflections.

A complete description of a mixed-layered clay mineral requires identification of the types of layers involved (e.g., illite and smectite), the proportions of each, and the type of order or lack thereof in the stacking sequence of the two-layer types along the Z direction (the Reichweite; see Chapter 5, p. 173). We limit the discussion here to two-component systems because multicomponent interstratification seems to be exceedingly rare in sedimentary rocks. In addition, consideration is given only to illite, smectite, vermiculite, kaolinite, chlorite, and serpentine (Al-lizardite and bertherine). These mixed-layered mineral components are those that the shale petrologist is most likely to encounter.

The easiest mixed-layered clay minerals to identify contain two components in equal proportions with R1 ordering. Such minerals have been assigned mineral names and can be thought of as non-mixed-

layered minerals that have unit cells whose 001 spacings are equal to the sums of 001 spacings of the two components involved. Large cells such as these are called *superstructures*, and it is convenient to designate their spacings as $d(00l)^*$. (This asterisk should not be confused with the symbol for reciprocal space, which is a widely used mathematical device in X-ray crystallography.) Diffraction patterns for well-oriented samples of these two-component systems consist of a set of basal reflections whose spacings follow the Bragg law, $d = d(001)^*/l$, where l is the integral order. If this relation is closely obeyed, the pattern of peaks is called *rational*. Corrensite is a common example, one type of which is made up of equal molecular proportions (50/50) of chlorite and smectite unit cells that are stacked in perfect alternation (*R1*). You might question whether corrensite should be considered a mixed-layered clay mineral, given its regular structure and rational pattern. After all, pure chlorite consists of a regular alteration (in 50/50 proportions) of silicate (talc-like) and hydroxide (brucite-like) “unit cells,” yet we usually do not think of chlorite as an interstratified mineral that consists of talc and brucite. Mineral species such as corrensite, however, need to be placed somewhere, and traditionally they are included with the mixed-layered clay minerals.

Other mixed-layered clay minerals do not share such rigid structural constraints. In these, proportions of end-members are not equal, and ordering may be imperfect. Consequently, randomness occurs in the stacking sequences, leading to structures that can be described only statistically. The stacking sequences in such structures, therefore, are not periodic, and, as you might expect, they produce aperiodic 00 l diffraction patterns. These patterns we call *irrational*. Irrationality is evidence of some randomness in the interstratification, and the approach to rationality is quantified by the percent standard deviation about the mean of a set of $d(001)$ values calculated from the various reflections. The number is reported as the coefficient of variation

Table 8.1. Coefficient of variation for 00 l diffraction patterns of EG-corrensite and of randomly interstratified chlorite/EG-smectite containing 70% chlorite

Corrensite			Chlorite/EG-smectite		
l	d	$l \cdot d(001)^*$	l	d	$l \cdot d(001)$
1	31.31	31.31	1	15.29	15.29
2	15.73	31.46	2	7.41	14.82
4	7.78	31.12	3	4.74	14.22
5	6.23	31.15	4	3.49	13.96
6	5.19	31.14	5	2.83	14.15
7	4.46	31.22	7	2.05	14.35
8	3.89	31.12	9	1.56	14.04
9	3.46	31.14			
10	3.11	31.10			
Mean		31.20			14.40
CV		0.38%			3.34%

(CV). By definition (Bailey, 1982), values $< 0.75\%$ define a mineral that qualifies for a specific name, such as corrensite. If $CV > 0.75\%$, the structure is sufficiently aperiodic to limit the designation to mixed-layered nomenclature, such as chlorite/smectite. Table 8.1 shows CV values for corrensite and for a randomly interstratified chlorite/smectite.

The corrensite spacings follow the Bragg law as well as can be expected, given the usual inaccuracies in measuring d . On the other hand, the diffraction pattern of randomly interstratified chlorite/smectite is demonstrably irrational and can be confidently ascribed to a mixed-layered species with at least some randomness in the stacking sequence. The test, which is easy to apply, is definitive—

if you are certain that all peaks considered belong to the same mineral species. Let us see why some types of mixed-layering produce irrational patterns.

MÉRING'S PRINCIPLES AND MIXED-LAYERED NOMENCLATURE

The model conceived by Méring (1949) provides the best insights into the character of mixed-layered clay mineral diffraction patterns. According to this concept, reflections occur between the nominal positions of the $00l$ peaks of both members of the mixture, and the positions of these intermediate reflections are fixed by the proportions of the end-members in the interstratification. The observed reflections are thus composites, or compromises, of the positions and, to a certain extent, the intensities of two end-member reflections. For the example of illite/EG-smectite, a reflection will be present between the illite 002 and EG-smectite 003 ($15.8^\circ 2\theta$) peak positions, and it is labeled the illite/EG-smectite 002/003. Remember, you will not see these end-member reflections in the diffraction pattern; they simply represent diffraction components that together produce a maximum. The maximum is broad if end-member reflections are far apart and sharp if they are close together. The diffraction pattern is usually unlike that of either of the end-members. The diffractogram for randomly interstratified clay minerals thus differs from that of a normal clay mineral in two important respects: (1) members of the set of so-called $00l$ peaks do not have the same breadths, and (2) the reflections have irrational spacings.

Our nomenclature for mixed-layered clay minerals is as follows. We name a mineral by listing the species with the smallest $d(001)$ (in the natural state) first and separate the names with a slash. For example, mixed-layered illite-smectite is called illite/smectite (IS or I/S, as you may find in the literature). The mineral name is preceded by the Reichweite, which describes the ordering type (see Box 5.3, p. 173), and a number in parentheses following the first name gives the decimal fraction of that type in the mixed-layered mineral. For example, the designation *R1 illite(0.7)/smectite* means a composition of 70 mol % illite with 30 mol % smectite. The layer types are

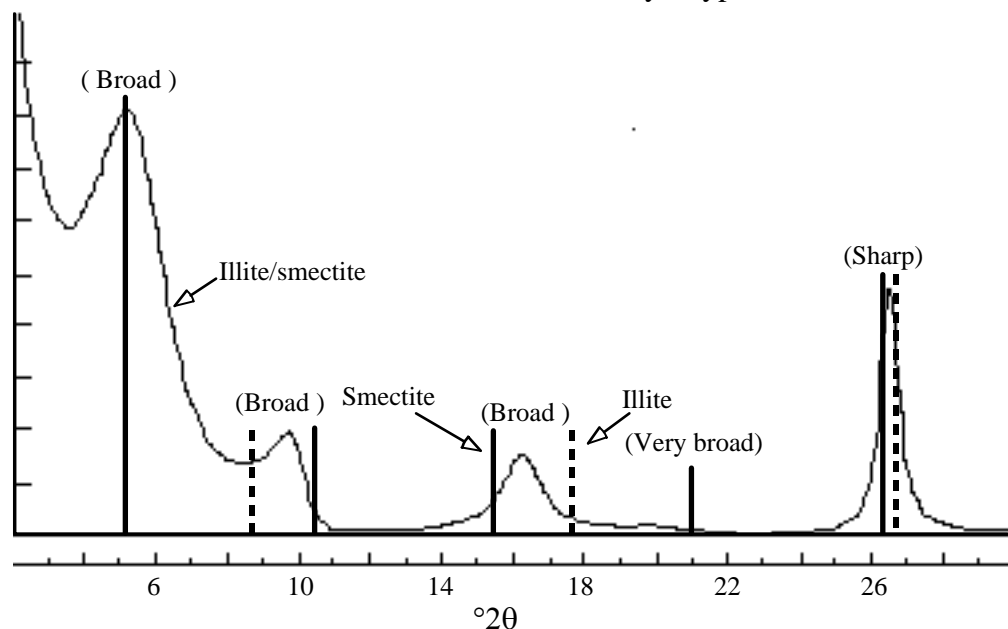


Fig. 8.1. *R0 illite(0.5)/EG-smectite* and the locations of the $00l$ reflections for illite and smectite.

stacked along Z in such a way that smectite layers never follow smectite layers.

Figure 8.1 demonstrates Méring's principles. The continuous profile illustrates a randomly

interstratified (*R0*) illite/EG-smectite, 50% illite. Using the terminology given above, this becomes *R0* illite(0.5)/EG-smectite. The solid vertical bars mark the positions of the smectite 00*l* reflections, and the broken bars designate the same for illite. Peaks whose positions depend on the proportions of illite and smectite occur near 10° 2θ for the composite illite 001 and EG-smectite 002 reflections and 16° for the illite 002 and EG-smectite 003 reflections. What reflections do you think contribute to the peak at 26.6° 2θ? Notice that the “peak” near 20° 2θ is very weak and broad. It is formed by the composite of the illite 002 and the smectite 004 reflections (the 002/004), which are widely separated. The reflection near 16° 2θ is stronger, yet also quite broad because it is a composite of the illite peak near 17.8° and the smectite peak near 15.8° 2θ. On the other hand, the peak near 26.6° 2θ owes its sharpness to the close juxtaposition of the illite 003 and the smectite 005 reflections. Note that a strong but broad reflection occurs at 5.2° 2θ at the smectite 001 position. The smectite 001 is not displaced because no illite peak is nearby. Instead, it becomes progressively broader and weaker as the proportion of illite increases.

Ordering causes the appearance of new reflections containing components of the 00*l* series of the superstructure. Figure 8.2 compares diffraction patterns for EG-K-rectorite (dashed line) and *R1* illite(0.7)/smectite. The patterns are similar except for some peak displacements, line breadths, and the near disappearance of the superstructure 001* reflection for the 70% illite pattern. The position of 001* is marked only by a slight change in slope of the “background.” Think of the 70% composition as a random interstratification of *rectorite* with enough illite layers to bring the composition from 50% illite to 70% illite. The 002* is weakened and broadened for two reasons. First, the rectorite component is less abundant than it was in the 50/50 composition, and, second, interference between the 002* and the illite 001 reflections has broadened the composite diffraction reflection, thus reducing its height. This ordered example contains some randomness in the stacking sequence along the Z axis because some smectite layers are separated by more than one illite layer. *Randomness must be present if the mineral contains component proportions that differ from 50%. But there need not be ordering at the 50/50 composition.*

If you think about the peak positions for the 70% composition, they will make sense. Figure 8.2 has vertical lines that depict the positions of the illite 001 and 002 reflections. The second-order superstructure reflection (002*) at about 6.6° 2θ has been displaced slightly toward the illite 001 position, and the 003* has moved in the opposite direction, also because of interference with the illite 001 peak. The K-rectorite 005* reflection (the 004* and 006*

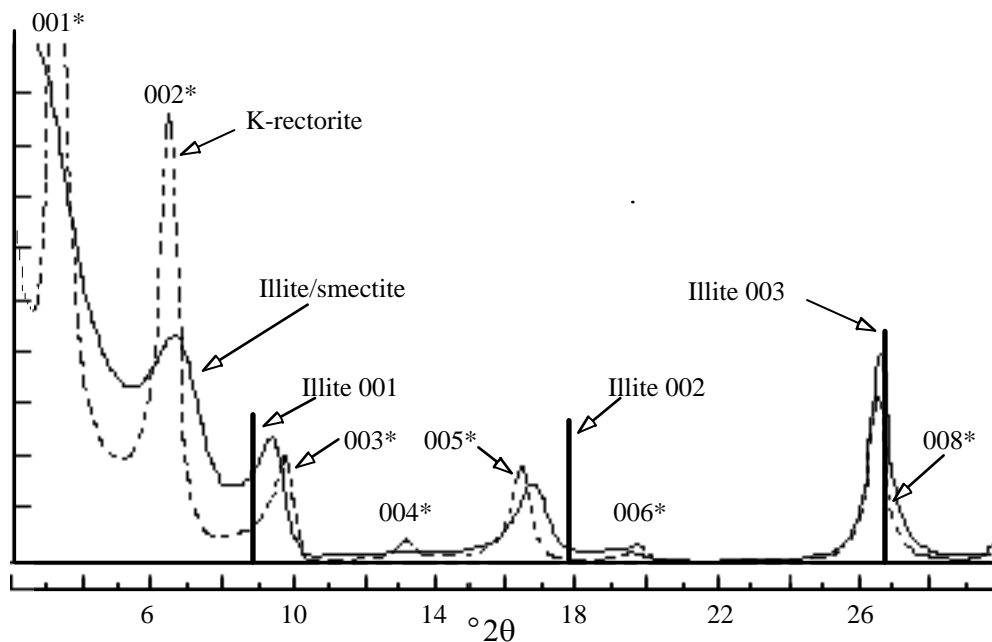


Fig. 8.2. *R1* illite(0.7)/EG-smectite and EG-K-rectorite[*R1* illite(0.5)/EG-smectite] and the positions of the peaks for pure illite.

are barely visible) near $16.2^\circ 2\theta$ has been similarly affected by proximity to the illite 002 and lies near 16.8° (the 002/005* reflection) for the 70% composition. The illite 003 is almost coincident with the K-rectorite 008* reflection, so the peak near 26.6° is essentially unaffected. With increasing illite content, the superstructure peaks that are far from the illite reflections (the 001*, 002*, 004*, and 006*) become progressively weakened, and the other reflections migrate toward the nominal positions of the pure illite pattern. You will be able to see how these principles operate in the following discussion of the diffraction patterns of mixed-layered clay minerals.

The Q Rule, a Broadening Descriptor

The different line breadths that are evident in Fig. 8.1 are quantifiable, and indeed, we can invent a rule for detecting small amounts of interstratification—amounts so small that they can escape detection by a consideration of peak positions. The rule is a quantification of Méring's principles. It works this way. Suppose that small (a few percent) amounts of mica are suspected in a chlorite. Simply take the ratio of the mica $d(001)$ divided by the chlorite $d(001)$, or in this case, $10/14.2 = 0.704$, and multiply this ratio by the l values for the chlorite reflections (Table 8.2). Then for each such value, calculate the deviation from the nearest integer and call the result Q . The values for Q predict the different line breadths. In this example, the broadest of the "chlorite" reflections will be the 002 and 005, and the 003, 007, and 00,10 will be sharp. A Q value of 0.000 designates a reflection that has no mixed-layered broadening, that is, the line breadth is controlled only by crystallite thickness (and instrumental effects). A value of 0.5 identifies a peak that has the maximum breadth possible for that mixed-layered mineral.

Figure 8.3 shows a plot of these Q values versus the calculated line breadths for a randomly interstratified *R0* biotite(0.1)/chlorite. The line breadths have been multiplied by $\cos\theta$ to eliminate angle-dependent particle-size broadening, e.g., see the Scherrer equation, Eq. (3.8), p. 87. For the calculated pattern, a mean defect-free distance of 10 unit cells was used in conjunction with a maximum

crystallite thickness of 50 unit cells (see Eq. A.8 and related discussion, p. 370). The calculated data show some scatter and the curve is not quite linear, but nevertheless you can see that Q is well correlated with line breadth. The broken line on Fig. 8.3 shows the approximate relation for R0 biotite(0.5)/chlorite. Suppose that the chlorite contained no biotite at all. Then a plot of Q versus line breadth would yield points distributed along a line parallel to the vertical axis of Fig. 8.3 because all the peaks would have identical breadths (Q ceases to have any meaning for such a case), and these are controlled by particle size broadening, the angular dependence of which has been removed by multiplying each of the line breadths by $\cos\theta$. We conclude that the *slope* of the curve of Fig. 8.3 can be used to estimate the proportion of biotite in a mixed-layered biotite/chlorite. Such a slope-composition relation is highly nonlinear with greatest sensitivity at small

Table 8.2. Calculation of the broadening descriptor, Q

Order	Order x 0.714	Q
1	0.704	0.296
2	1.408	0.408
3	2.113	0.113
4	2.817	0.183
5	3.521	0.479
6	4.225	0.225
7	4.930	0.070
8	5.634	0.366
9	6.338	0.338
10	7.042	0.042

contents of one of the interstratified species. A few percent or less of a minor component can be identified and estimated by this method, and such a small amount might escape detection if you paid attention only to peak positions. Note—in the extreme example given here (reflections out to the chlorite 00,10), you would have to correct the experimental data for instrumental effects, most importantly, for $\text{CuK}\alpha_1$ - $\text{CuK}\alpha_2$ broadening.

The relation between Q and line breadth needs calibration by means of known standards (unlikely) or from calculated line breadths, which can be obtained, as in the example of Fig. 8.3, from NEWMOD[©] (Reynolds, 1985). The Q principle is also useful for the *identification* of mixed-layered clay minerals. Suppose you suspect that your sample contains a paragonite [$d(001) = 9.7 \text{ \AA}$] interstratified with very small amounts of 2-water-layer smectite [$d(001)=15 \text{ \AA}$]. You could verify this identification by a measurement of the line breadths.

The absolute line breadths of all the reflections must be correctly modeled if line broadening is used for a quantitative analysis of layer proportions. If the discussion above dealt with a mineral of much smaller or larger crystallite thickness, the slope of the line on Fig. 8.3 would be different, and for very thin

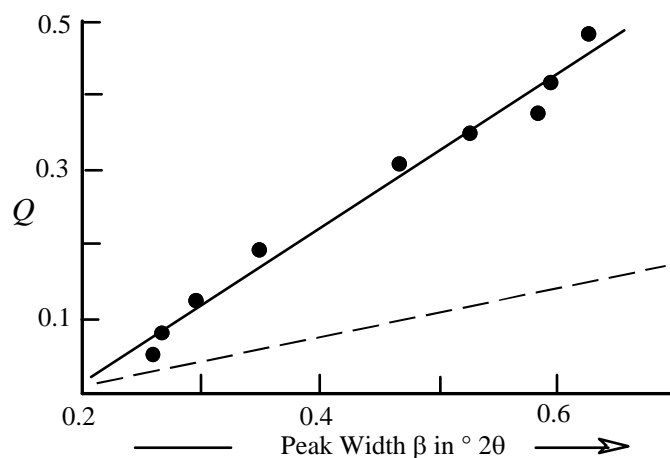


Fig. 8.3. The correlation between Q and line-breadth for R0 biotite(0.1)/chlorite. The broken line locates the relation for R0 biotite(0.5)/chlorite.

crystallites, the scatter of points about the line would be increased. Think of the breadth of a large- Q peak as a composite of mixed-layered broadening and crystallite thickness broadening. The mixed-layered component is fixed for a given layer proportion, but the crystallite size component becomes large for thin crystallites and overwhelms the mixed-layered effect. There are always errors in the measurement of peak breadth, and at some level of small crystallite size, the additional effect of mixed layering on peak breadth disappears in the experimental error. Alternatively, the Q rule works best for very thick crystallites because most of the breadth of large- Q reflections is due to mixed-layered broadening.

The rationale behind the meaning of Q is as follows. If Q is very small, it means that a reflection from one interstratified component is almost superimposed on a reflection from the other component, and as Méring's rules tell us, that results in a sharp reflection. If Q is 0.5, that means that the reflection whose order is indicated by the "Order" column in Table 8.2 is equidistant from two flanking orders of the other component, and that causes maximum line broadening.

Let's see what can be done with line broadening in a more exhaustive application. Figure 8.4A shows three experimental diffraction patterns of chlorite that has been (1) heated at 250°C and analyzed in an enclosed chamber through which was streamed tank nitrogen to maintain dehydration (Chapter 6); (2) solvated by EG; and (3) analyzed in the air-dried condition. The data were obtained with two Soller slits and a 0.05° detector slit to minimize instrumental broadening. A thick slide of a well-oriented specimen was used in conjunction with long count times for the step scan procedure, producing a pattern with a high peak-to-noise ratio.

Some shift is noticeable among the 002 reflections of the three patterns, but one would be hard put to assign a quantitative value to any smectite present. (The EG-treated preparation shows a superstructure reflection that indicates the physical admixture of a small amount of corrensite, but the strengths of corrensite's other reflections are insufficient to affect the chlorite peaks very much.) Peak breadths for all the chlorite reflections from the three preparations were measured as the width, in ° 2θ , of the peaks at half-height. These measurements were made from plots of the diffraction patterns at greatly expanded horizontal scales. Trial and error calculations were performed by NEWMOD[®] for different values of the distribution of N values (the number of unit cells in coherent scattering array) and percent randomly interstratified smectite, and the same values for each of these were applied to all three final model structures.

Figure 8.4B shows comparisons between experimental and calculated (model) line breadths for five reflections from each of the three preparations. The agreement between experiment and model is excellent, and a conclusion based on 15 reflections gives confidence that the procedures used are valid and that the amount of smectite interstratified with this chlorite must be very close to 7%. Notice that for some preparations, the differences in breadths are

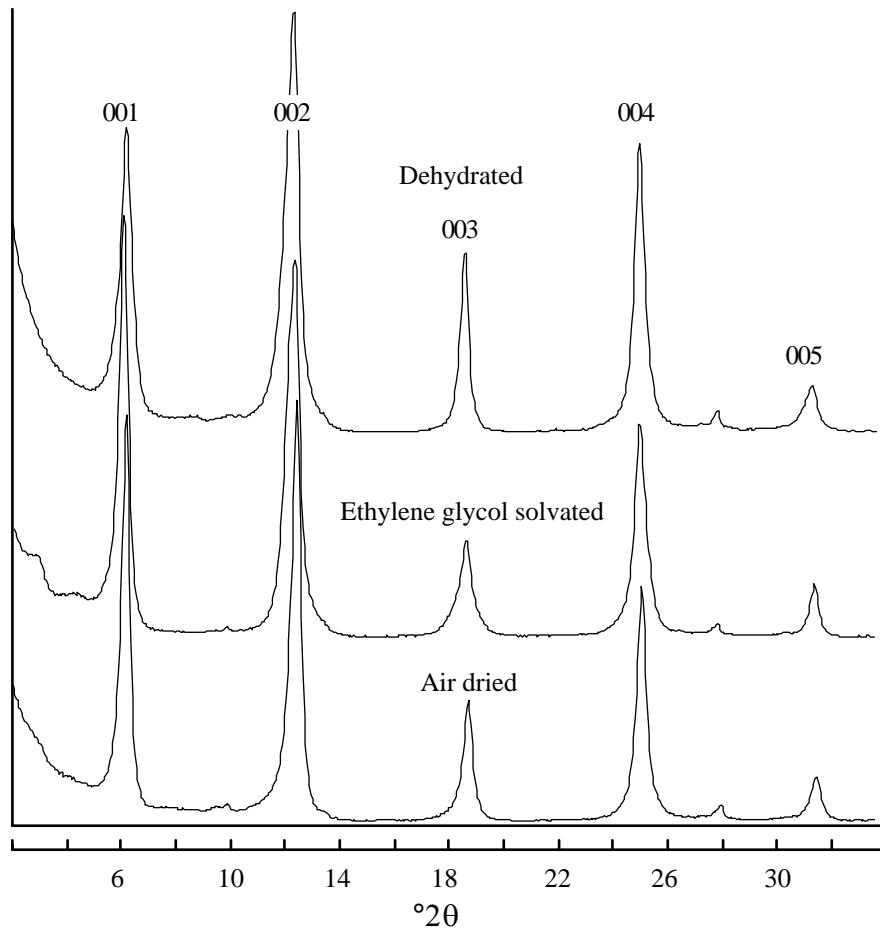


Fig. 8.4A. Experimental diffraction patterns for different preparations of a chloritic mineral.

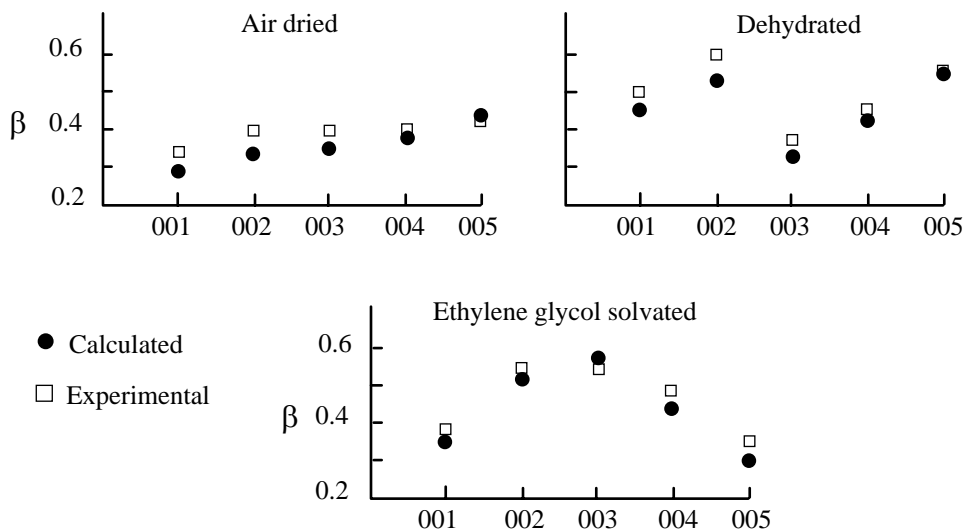


Fig 8.4B. Comparisons between experimental and calculated line breadths (β) for different diffraction orders of the preparations shown by Fig. 8.4A.

as large as a factor of two, and that differences between all peak breadths are much larger than the error of measurement which is estimated to be $0.02^\circ 2\theta$. These observations suggest that we could go to much smaller proportions of smectite and still quantify the result—say, down to 2% if the instrumental

contributions to the peak breadths were removed by deconvolution procedures.

The line-broadening method of analysis cannot be used for compositions that exceed about 10% to 15% of one component unless the interstratification is random. In any event, the peak position method is the one to use for compositions nearer the middle of the range. A *caveat* is in order here. The mineral line breadths can be swamped by instrumental broadening if the diffractometer is poorly focused (one Soller slit, large detector slit, large beam slit, or misalignment). A refined quantitative analysis of mixed-layering based on line breadths may require that instrumental broadening effects be removed mathematically from the diffraction profiles by the process of deconvolution (see Klug and Alexander, 1974), and that is beyond the scope of this text, though it is not particularly complicated or time consuming even with PC-type computers. For many applications, however, it is sufficient to use two Soller slits, a 1° beam slit, and a 0.05° (or smaller) detector slit and to limit the analysis to the lower diffraction angles (<40° 2θ), where $K\alpha_1/K\alpha_2$ broadening is minimal.

The successful application of Méring's principle in this rigorous manner suggests that it has a fundamental reality that has not been generally appreciated. It is impressive what the great ones were able to do without computers.

MIXED-LAYERED CLAY MINERALS

Illite/Smectite

Illite/smectite is the most abundant, diverse, and widespread of the mixed-layered clay minerals in sedimentary rocks and soils. You will need to become proficient in identifying it in all its structural ramifications if you intend to do much work on clay minerals from soils or rocks. The best method of analysis is to study and compare diffraction patterns produced from both air-dried and EG-solvated preparations.

Most of the attention here is given to the interpretation of diffraction patterns obtained from EG-solvated specimens because these patterns are the most diagnostic. For patterns from the air-dried condition, we assume that a smectite interlayer contains two planes of water molecules coordinated about exchangeable Ca ions, producing a smectite $d(001)$ of 15 Å. Unfortunately, the basal spacing is a fairly sensitive function of ambient humidity and the type of exchange cation. Thus, unless you saturate your samples with Ca and maintain strict control of humidity (a difficult thing to do), you should not use peak positions from air-dried preparations to obtain composition estimates. Air-dried sample data are important to use as baselines from which to observe the changes brought about by EG solvation.

Suppose that diffraction patterns are recorded from a mixed-layered clay mineral in both the air-dried and EG-solvated conditions. When you see that EG solvation has caused significant changes in the diffraction pattern, a smectite component is surely present, because EG solvation has little effect on vermiculite, and other likely layer types are not affected at all by this treatment. So you have a "something"/smectite, and that something may be illite, chlorite, kaolinite, talc, serpentine, vermiculite, etc. The interstratification is random and probably rich in smectite if EG solvation produces a peak near 5.2° 2θ. Concentrate now on the EG-solvated case. Examine the region near 16 to 17.7° 2θ, and if you note a reflection there (the 002/003), the diagnosis is likely illite/smectite. You can estimate the proportion of illite from the data in Table 8.3, which have been tabulated from calculated diffractograms for each specific composition. If you want to work with only one reflection, the peak near 17° 2θ is the best choice. The peak near 9° is more sensitive to shifts caused by small crystallite size.

You can confirm your qualitative identification of the mixed-layered species by heating the sample to 375°C for 1 h. The diffraction pattern should resemble a pure illite (10 Å structure) with a relatively weak 003 reflection.

The quantity $\Delta 2\theta$ (Table 8.3) is useful because, for some mixed-layered minerals, it is the most “robust” descriptor of composition, as the mathematicians say. Š rodoń (1980) has demonstrated the power of differential 2θ measurements for accurately estimating the composition of illite/smectite. His procedures involve several reflections and require very good diffraction patterns free from peak interferences.

The advantages of using $\Delta 2\theta$ are several. It is a differential measurement; therefore, results based on it are relatively insensitive to goniometer zero-alignment problems and specimen displacement errors. The latter are very likely despite your best efforts. For illite/smectite and some other mixed-layered clay mineral analyses, the sensitivity of the composition estimate is enhanced because the two peaks involved in the measurement move in opposite directions as the composition changes. Finally, analytical errors caused by sample-to-sample variations in the thickness of the EG interlayer in smectites (Š rodoń , 1980) are at least minimized by the use of $\Delta 2\theta$ because changes in EG thickness cause both reflections to be displaced in the same direction. The differential 2θ value is thus relatively unaffected by variations in thicknesses of the interlayer solvation complex.

Let us now see how all this is applied to the diffraction pattern shown in Fig. 8.5. EG solvation has produced a strong but broad reflection near $5^\circ 2\theta$ ($d = 17 \text{ \AA}$). A good guess at this point is that you have a randomly interstratified illite/smectite. The other peak positions, near 9° and $16^\circ 2\theta$, support this supposition. Quantify the result using their positions (Table 8.3). You could make a better estimate of composition, using the $\Delta 2\theta$ value in Table 8.3, assuming that interferences from other clay minerals do not make this measurement impractical.

Figure 8.6 shows diffraction patterns for *R1* illite(0.7)/smectite. Again, concentrating on the EG-solvated case, the high-angle portion of the pattern is similar to the random case in Fig. 8.5, except that the peaks are sharper for the ordered structure. Most important, a strong reflection is present at low diffraction angles ($6.5^\circ 2\theta$, 13.3 \AA) that contains a dominating component of the second-order superstructure reflection (002^*). This reflection should shout ORDERING! to you. *The interpretive importance of the low-angle region cannot be overemphasized.* A reflection at $5^\circ 2\theta$ indicates random interstratification, and one near $6.5^\circ 2\theta$ indicates *R1* ordering. The latter reflection becomes broad and weak and does not move very much as the composition becomes more illitic.

A noticeable peak at angles between 7 and $8^\circ 2\theta$ (about 8° in Fig. 8.7) indicates long-range ordering, that is, Reichweite values greater than unity. Figure 8.7 shows a calculated pattern for *R3* illite(0.9)/smectite. In the EG-solvated state, the broad shoulder at $8^\circ 2\theta$, or $d = 11.1 \text{ \AA}$, contains components of the illite 001 reflection and of the fourth order of a 47 \AA superstructure peak whose unit cell consists of three 10 \AA illite layers and one 17 \AA EG-smectite layer. The reflection is called the $001/004^*$. This peak is diagnostic for long-range ordering, that is, $R > 1$. It denotes the presence, in the mixed-layered crystallites, of the frequent unit cell sequence ISII mixed with additional illite layers.

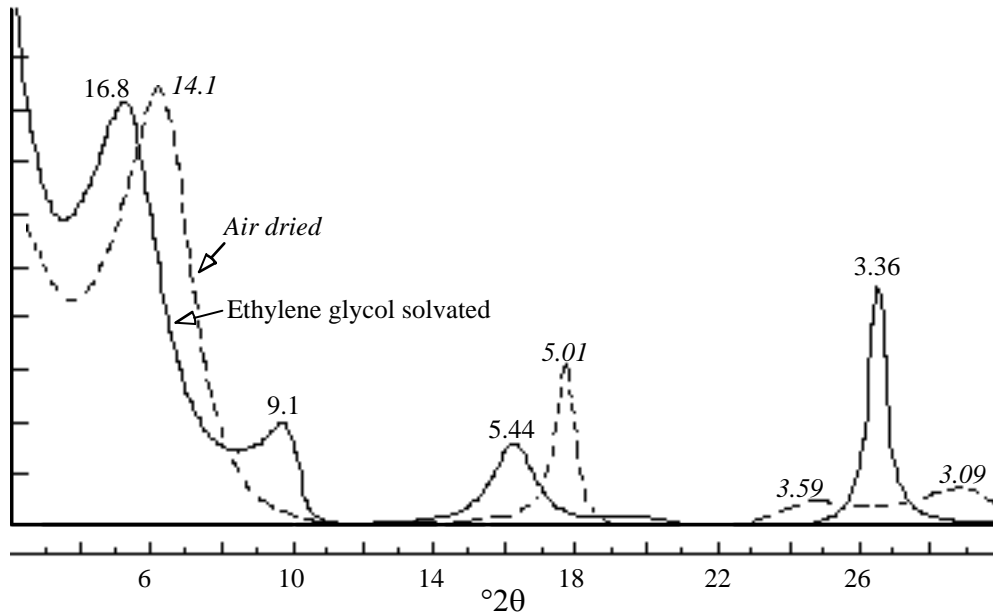


Fig. 8.5. EG-solvated and air-dried *R0* illite(0.5)/smectite.

We draw three conclusions that are crucial to the correct identification and description of mixed-layered illite/smectite.

1. The diffraction patterns of air-dried illite/smectite are altered significantly by solvation with EG, and such behavior leads to the provisional identification of illite/smectite. Heating to 375°C for 1 h provides confirmation of the identification; the result is a diffraction pattern similar to that of illite.
2. The Reichweite (ordering type) is determined by the position of the reflection between 5 and 8.5° 2θ for EG-solvated preparations.
3. Percent illite can be determined by the position of the reflection near 16 to 17° 2θ, but a better way is to base the estimate on a value for $\Delta 2\theta$ (Table 8.3).

Characterization of I/S is routine and definitive if you are armed with high-quality diffraction patterns from air-dried, EG-solvated, and dehydrated preparations of a pure I/S sample. Interpretations of poor patterns from mineral mixtures are another matter. Mixtures of discrete (detrital?) illite with I/S in shales are the norm, and if the I/S is illite-rich, the criteria described above are difficult to apply. Figure 8.8 shows air-dried and EG-solvated simulations of *R1* illite(0.65)/smectite mixed with 40 wt % illite. The top and bottom traces are typical calculated patterns. The two middle traces were prepared by superimposing the calculated traces on a noisy background produced by a pseudorandom number generator. These are meant to show the effects of the pattern degradation that results from poor (average?) laboratory procedures.

Table 8.3. The positions (CuK α) of useful reflections for estimating percent illite in illite/EG-smectite

001/002

002/003

% Illite	Reichweite	$d(\text{\AA})$	$^{\circ} 2\theta$	$d(\text{\AA})$	$^{\circ} 2\theta$	$^{\circ} \Delta 2\theta$
10	0	8.58	10.31	5.61	15.80	5.49
20	0	8.67	10.20	5.58	15.88	5.68
30	0	8.77	10.09	5.53	16.03	5.94
40	0	8.89	9.95	5.50	16.11	6.16
50	0	9.05	9.77	5.44	16.29	6.52
60	1	9.22	9.59	5.34	16.60	7.01
70	1	9.40	9.41	5.28	16.79	7.38
80	1	9.64	9.17	5.20	17.05	7.88
90	3	9.82	9.01	5.10	17.39	8.38

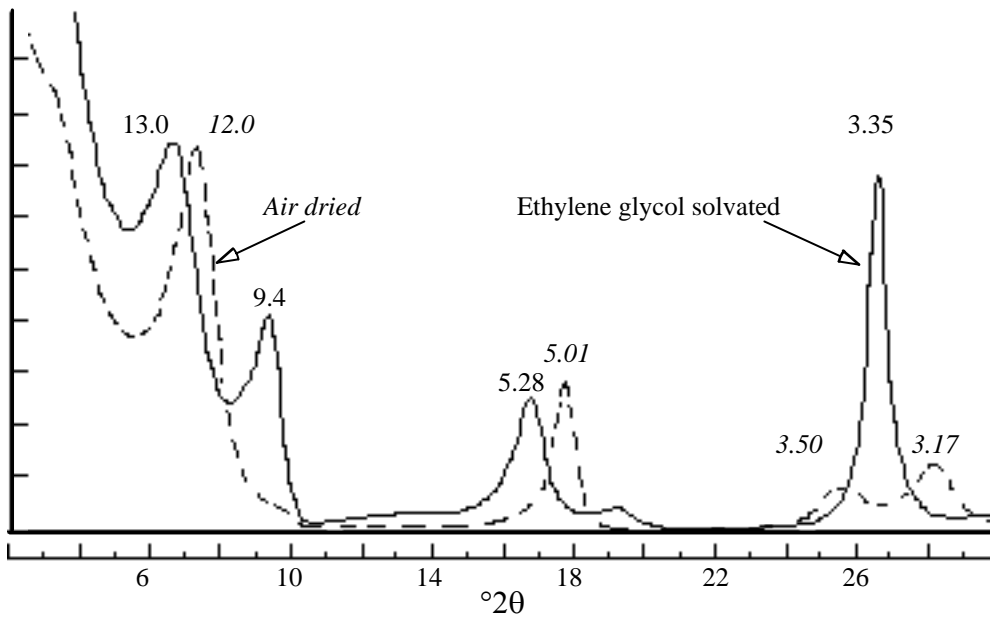


Fig. 8.6. EG-solvated and air-dried R1 illite(0.7)/smectite.

First of all, how do we know that I/S is present? Well, the hypothetical sample has responded to EG solvation, so it certainly contains an expandable component. Notice the very sharp and intense reflection near 17.7° for the air-dried structure. The character of this peak is due to the almost perfect superposition of the two-water-layer ($d = 15 \text{ \AA}$) smectite 003 component on the second-order illite contribution at 5 \AA ($Q = 0$). Thus both members of the

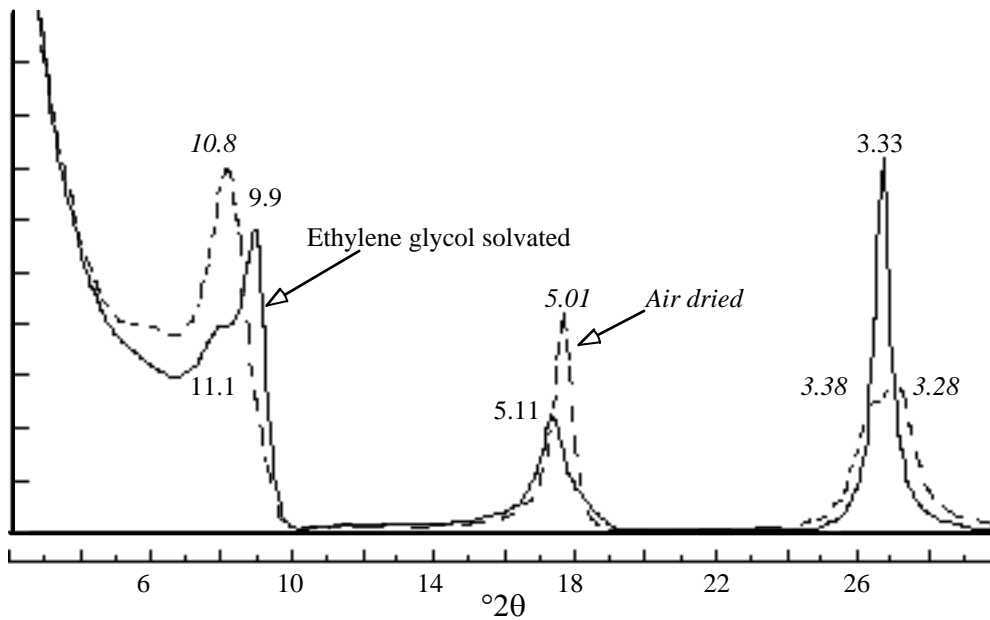


Fig. 8.7. EG-solvated and air-dried *R3* illite(0.9)/smectite.

interstratification have a peak there, so there is (1) no mixed-layered line broadening or distortion, (2) no peak shift, and (3) the amplitudes are additive. The discrete illite also has a peak at that position, which adds to the peak height but little to the breadth of the aggregate reflection. The aggregate peak becomes broad after EG solvation because the smectite 003 component is no longer coincident with the illite 002 position, resulting in mixed-layered broadening and a shift in peak position away from the 002 peak of the discrete illite. So, we are pretty sure that the sample contains I/S. Confirmation of the diagnosis is provided by the high-angle shoulder on the

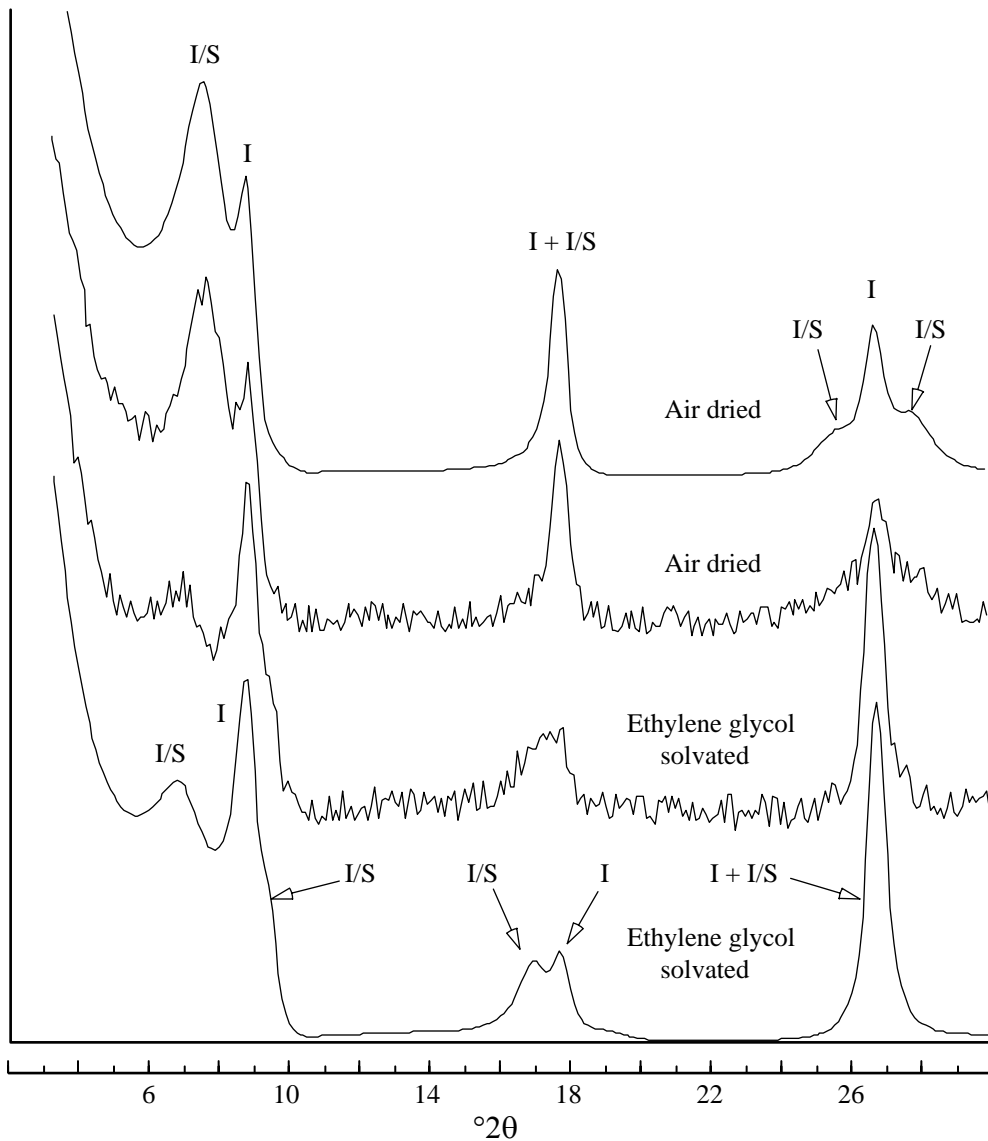


Fig. 8.8. Calculated patterns of EG-solvated and air-dried *R1* illite(0.65)/smectite mixed with 40 wt % illite. Shown are calculated patterns and the same patterns modulated by random noise to simulate poor data and the problems of analysis faced because of poor XRD tracings.

discrete illite 001 reflection that appears upon EG solvation. This unresolved mixed-layered reflection is the 001/002. You should become sensitive to the shape of the discrete illite 001 because if no I/S is present, the peak should be concave on the high-angle side; I/S of considerable expandability is present if EG solvation produces that bulge on the high-angle side, and an increase in the asymmetry of the illite 001 peak in the low-angle direction indicates the presence of I/S of low (10% or less) expandability.

The broad reflection near 6.7° that has shifted to that position with EG treatment can only be a strong component of the 002*—at least that is the only conclusion consistent with the other observations. Its position between about 6.6° and 6.8° indicates *R1* ordering, and its relatively low intensity, compared to the other unresolved I/S peaks, suggests that the I/S is illite-rich—perhaps between 20% and 35% expandable.

We can't do much more with this hypothetical sample if all we have are the two noisy diffraction patterns. We can't use the position of the 002/003 or the $\Delta 2\theta$ method because the required reflections are not resolved. We conclude that the I/S is *R1* ordered and contains between 20% and 35% expandable

layers.

Better diffraction patterns usually help a great deal in characterizing I/S in admixture with discrete illite, but not always. If discrete illite and/or I/S consists of very thin crystallites, then the peaks are broadened so much that problems of resolution remain regardless of the noise levels in the diffraction patterns. But at least if you work for high-quality patterns, you will be confident that you have all the information that can be obtained by XRD from any given sample.

Chlorite/Smectite and Chlorite/Vermiculite

Chlorite/smectite is the second most abundant mixed-layered clay mineral in sedimentary rocks and soils. Reported occurrences indicate that it lacks the diversity that we find in illite/smectite because structures with $R > 1$ and minerals that contain much more than about 50% smectite have not been identified with certainty, and even random structures seem to be limited to only slightly expandable compositions. In short, it seems that the majority of structures that you will encounter will be either $R1$ 50% chlorite compositions or $R0$ minerals with maybe 10% smectite layers or less. There is room for much disagreement here, but we will treat what we believe are the common types of chlorite/smectite: low-charge corrensite (chlorite/smectite) and chlorite/smectite, $R0$, > 50% chlorite. Unlike I/S, however, ordering type is difficult to ascertain if compositions are less than about 30% smectite, so ordered structures may be more common than we think.

Figure 8.9 shows diffraction patterns for low-charge corrensite (trioctahedral chlorite/smectite) in the air-dried and EG-solvated conditions. The 50/50 composition and $R1$ ordering produce a superstructure $d(001)^*$ of $14.2 + 16.9 = 31.1 \text{ \AA}$ for the EG-solvated case. Other peaks are positioned according to the Bragg law, and you can see the regular spacing of the various orders of reflection. The 003^* is missing because it is almost an extinction; i.e., the scattering amplitudes from the unit cell cancel out. The air-dried form also produces a rational pattern, and in this case the superstructure 001^* has a spacing of $14.2 + 15 = 29.2 \text{ \AA}$. In our experience, the single most diagnostic criterion for corrensite lies in the appearance, upon EG solvation, of the 004^* at about $11.3^\circ 2\theta$ or 7.8 \AA . This identifier is useful for typical samples that have interferences on many of the corrensite lines. (You might think, what about the superstructure reflection at very low diffraction angles? Isn't that definitive? The trouble is that there are several instrumental effects that can produce a spurious reflection there—the so-called “Texas Clay Peak,” among others—see D. R. Pevear for this terminology. If this very low angle peak is very intense, the diagnosis of corrensite is correct. If it is weak, beware of instrumental artifacts. Caution: calculated tracings of corrensite that deviate from 50:50 by as little as 2-3% sharply diminish the intensity of this peak, a possible reason that chlorite/smectite close to 50:50, but not corrensite, is seldom recognized.) Confirmation of a corrensite identification can be made by dehydrating the sample, causing the collapse of the smectite component to approximately 9.7 \AA , and leading to a new superstructure spacing of $9.7 + 14.2 = 23.9 \text{ \AA}$ (Fig. 8.10). As before, the spacings of the reflections produce a rational diffraction pattern, but now, the 001^* is absent.

Chlorite/vermiculite is a species closely related to chlorite/smectite. The difference between them detectable by X-ray diffraction methods is the extent of expansion when treated with EG or glycerol. In the air-dried condition, low-charge corrensite (chlorite/smectite) has a nominal $d(001)^*$ of 29.2 \AA that expands to 31.1 \AA upon EG solvation. The $d(001)^*$ value for high-charge corrensite (chlorite/vermiculite) is 28.6 \AA and is unaffected by EG solvation. Differentiation between the two minerals is based on quite small differences in peak position, which can be unreliable because the $d(001)^*$ values given here are nominal ones and there is a bit of variation from sample to sample. Heat treatments do not resolve the difficulties because the smectite and vermiculite components in the two collapse to approximately 10 \AA , particularly if the sample has been K-saturated. The best diagnosis is based on Mg saturation and *glycerol* solvation (Walker, 1957). The smectite component of

chlorite/smectite expands with this treatment to 17.7 Å, but vermiculite in chlorite/vermiculite remains at about 14.4 Å. Even these criteria can be ambiguous because some samples of chlorite/smectite absorb EG or glycerol very slowly, and days or weeks may be required for full expansion. A normal 12-h EG vapor treatment may, therefore, fail to disclose expansion and lead to the misidentification of chlorite/smectite as chlorite/vermiculite. To make matters worse, there may be interstratified expandable layers with charges that are intermediate between those of smectite and vermiculite, so a clean cut operational definition may be impossible.

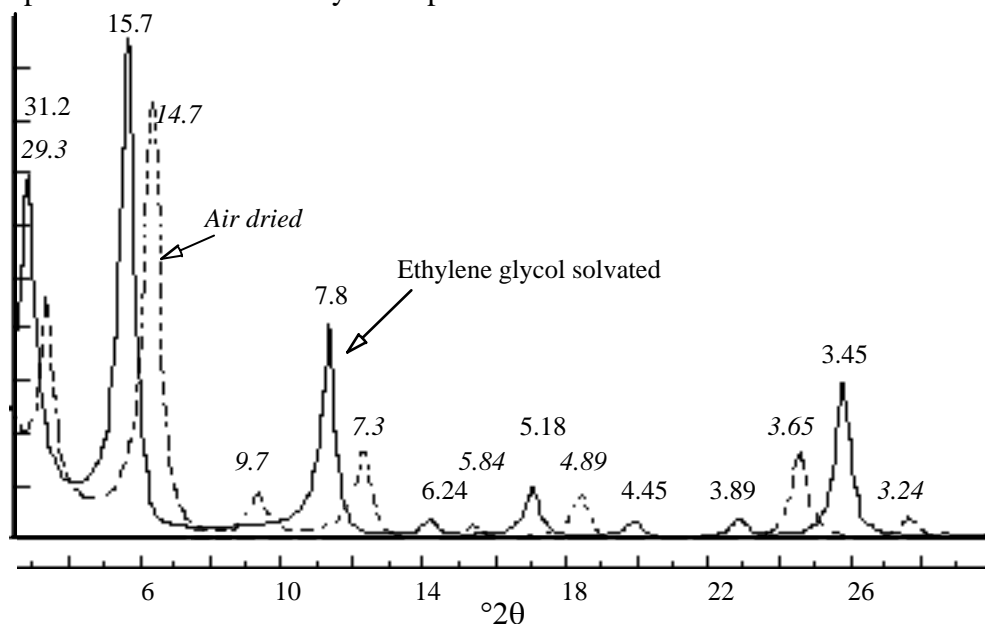


Fig. 8.9. Trioctahedral low-charge corrensite. All octahedral sheets contain 1 Fe per 3 sites.

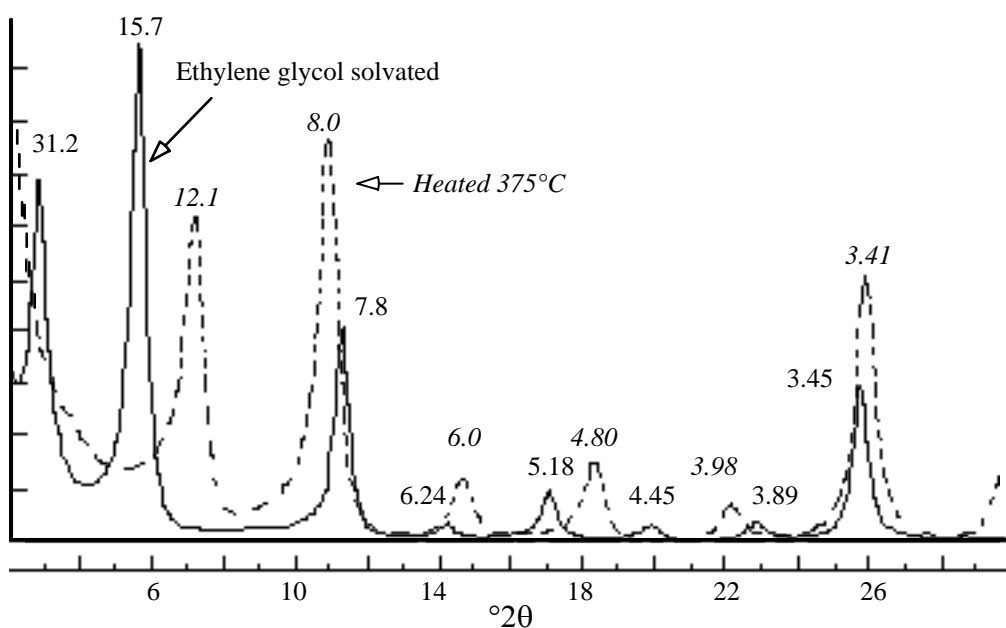


Fig. 8.10. Trioctahedral low-charge corrensite. All octahedral sheets contain 1 Fe per 3 sites.

The best advice that we can give is as follows: The mineral is chlorite/smectite if the diffraction pattern indicates expansion with EG; the result is indeterminate if EG solvation does not cause apparent expansion; chlorite/smectite is indicated if the sample shows expansion with Mg saturation and glycerol solvation; and the best diagnosis is chlorite/vermiculite if the diffraction pattern is essentially unaffected by this treatment.

Reported instances of chlorite/swelling-chlorite (Lippmann, 1956; Vivaldi and MacEwan, 1957) serve to cloud the picture further. Swelling-chlorite is such a poorly described phase that we have not attempted to calculate its diffraction characteristics. Just hope that any “corrensite” you encounter expands with EG solvation to about 31 Å and collapses (in the K-saturated form) to $d(001)^* = 24$ Å upon heat treatment. Figure 8.11 shows calculated patterns for R1 chlorite(0.5)/vermiculite in the air-dried condition and after heating. You should compare it to the corrensite of Figs. 8.9 and 8.10.

R0 chlorite(0.8)/smectite is shown in Fig. 8.12. The patterns superficially resemble chlorite except that the peaks have different breadths, the spacings are irrational, and solvation of the air-dried sample with EG has caused changes in the diffractogram. The relative intensities of the basal series depend on the content and location of the Fe substitution within the two possible chlorite octahedral sheets. The effects of Fe on intensity have been described for pure chlorite in Chapter 7. Confirmation of a chlorite/smectite diagnosis is provided by the diffraction pattern for the heated condition (Fig. 8.13). Notice that heating has caused sharpening of the reflection near 18.5°

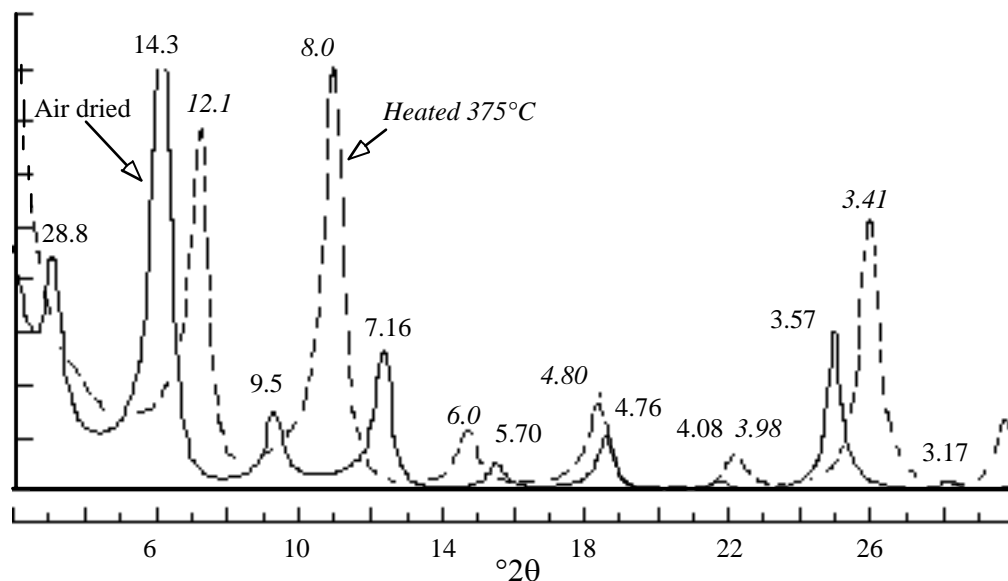


Fig. 8.11. Trioctahedral high-charge corrensite. All octahedral sheets contain 1 Fe per 3 sites.

2θ and migration of the 001/001 peak. The heat test is important for such minerals because of the possible misidentification of vermiculite/smectite as chlorite/smectite. Had the mineral been vermiculite/smectite, heat treatment would have collapsed the structure to about 10 Å and the diffraction pattern would have resembled that of either glauconite or illite.

The proportions of chlorite and smectite in mixed-layered chlorite/smectite can be estimated by the use of the data of Table 8.4. Again, we recommend the $\Delta 2\theta$ parameter for the best estimate of composition. Small (< 10%) amounts of smectite in smectite/chlorite are difficult to measure by peak migration characteristics, so the line-broadening analysis with application of the Q rule discussed earlier is the way to go for these compositions.

A common and vexing problem is identifying mixed-layered chlorite/smectite, of any type, in

samples that contain discrete smectite or chlorite or both, and these seem to be most (all?) samples. This difficulty doubtless is responsible for the controversy concerning the occurrence of mixed-layered chlorite/smectite whose composition is not near the 50/50 value that defines corrensite (see Hillier, 1995 and Robinson and Bevins, 1994, for opposite sides of this discussion). The minerals corrensite, mixed-layered chlorite/smectite, smectite, and chlorite have unit cells that in the air dried and EG-solvated states have thicknesses of approximately 14, 15, and 17 Å. These are similar enough to cause problems of multiple mineral peak

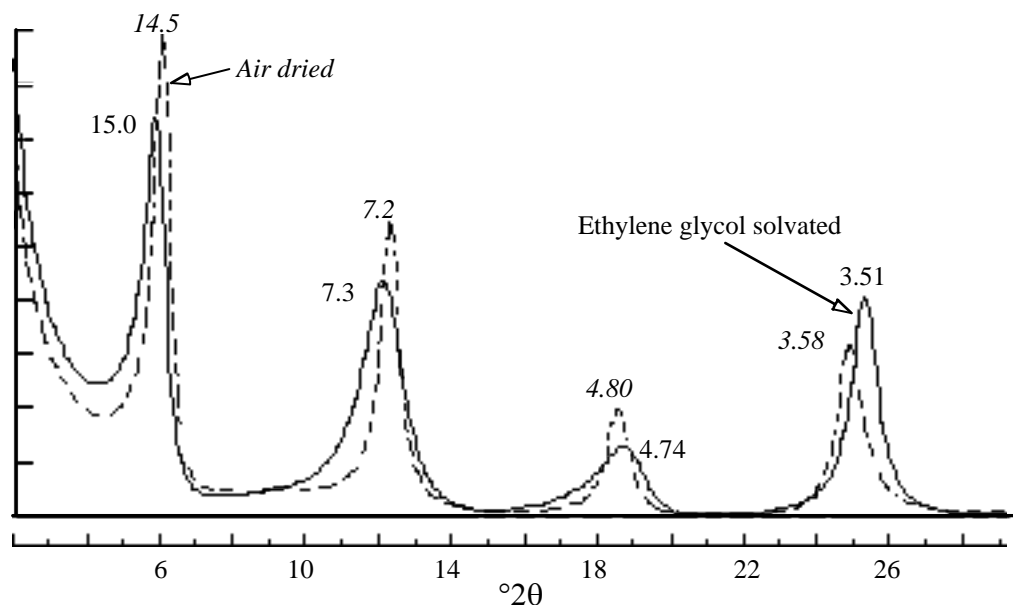


Fig. 8.12. R0 chlorite(0.8)/smectite, air dried and glycol solvated. All octahedral sheets contain 1 Fe per 3 sites.

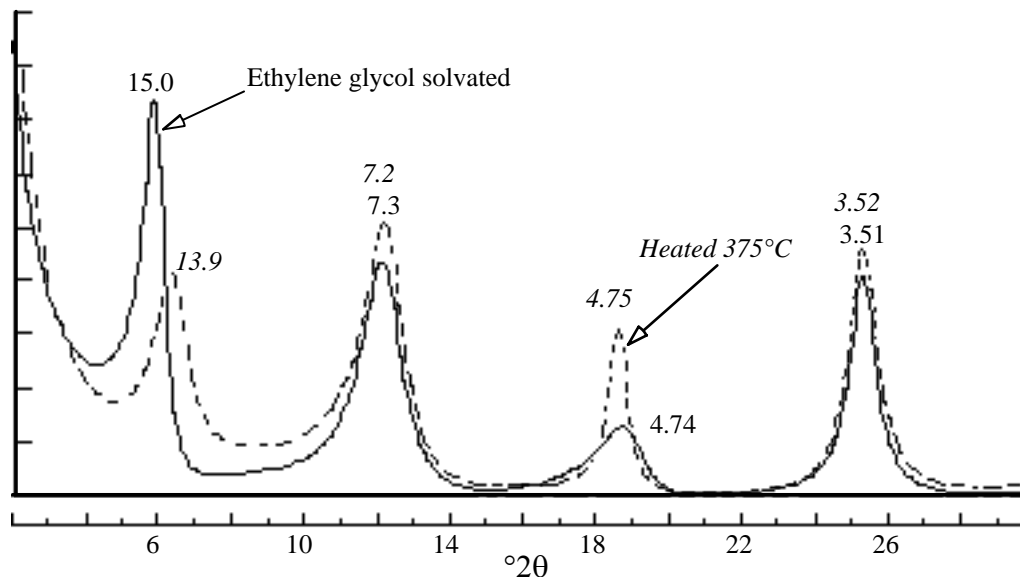


Fig. 8.13. R0 chlorite(0.8)/smectite, glycol solvated and heated to 375°C. All octahedral sheets contain 1 Fe per 3 sites.

resolution from such a mixture. But if the sample is dehydrated (heated for 1 h at 250°C in the Na-saturated condition) and analyzed in a stream of dry nitrogen to keep it dehydrated, expandable layers in the smectite and mixed-layered chlorite minerals are collapsed to about 9.6 Å, and that produces very

different looking diffractograms. Little can be learned from EG and air-dried preparations of these mineral mixtures.

Figure 8.14 compares experimental diffractograms from Ca-saturated EG-solvated and Na-saturated dehydrated preparations of the clay-sized fraction from a sample of the Point Sal ophiolite. The power of dehydration

Table 8.4. The positions (CuK α) of useful reflections for estimating percent chlorite in R0 chlorite/EG-smectite

% Chlorite	002/002		004/005		$\Delta^\circ 2\theta$
	$d(\text{\AA})$	$^\circ 2\theta$	$d(\text{\AA})$	$^\circ 2\theta$	
10	8.39	10.54	3.39	26.29	15.75
20	8.29	10.68	3.40	26.21	15.54
30	8.15	10.86	3.42	26.05	15.19
40	7.98	11.09	3.43	25.98	14.89
50	7.80	11.34	3.45	25.82	14.48
60	7.59	11.66	3.47	25.67	14.01
80	7.40	11.96	3.50	25.45	13.49
90	7.18	12.33	3.53	25.23	12.90

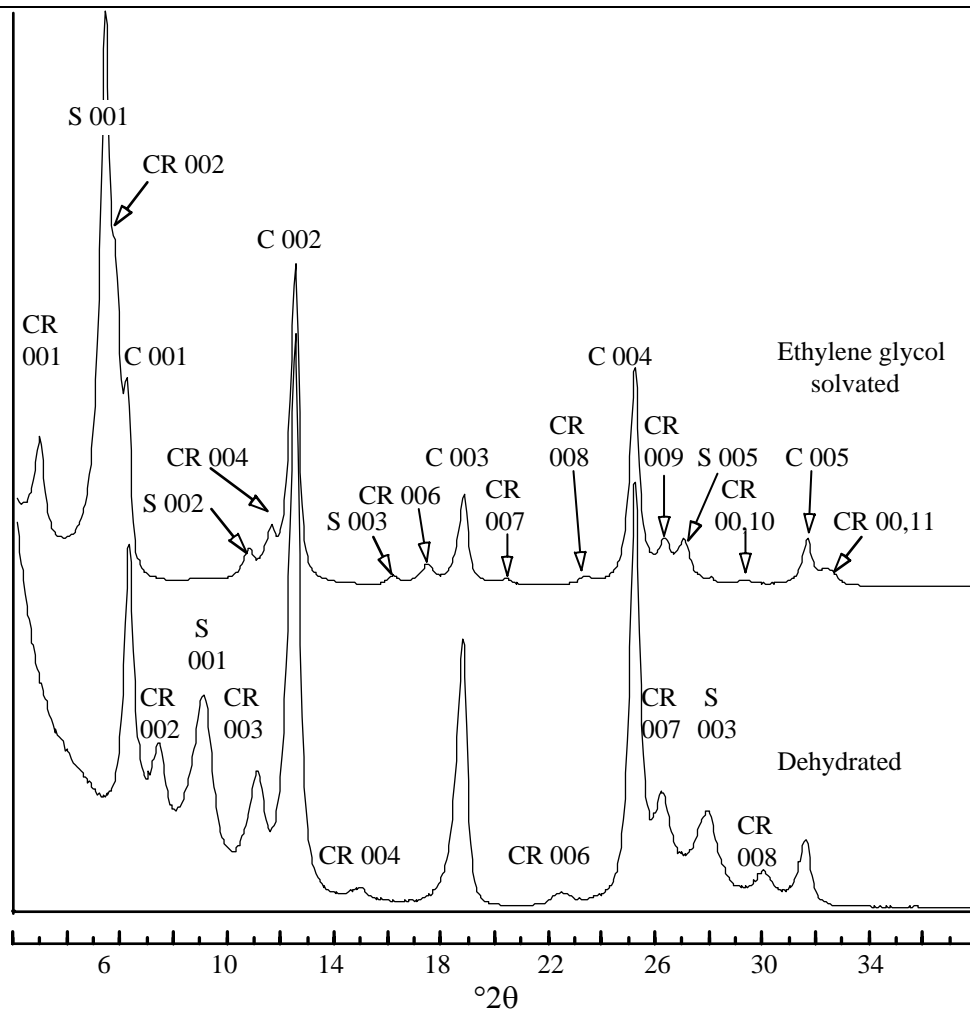


Fig. 8.14. Experimental diffraction patterns of a natural mixture of smectite, chlorite, and corrensite. Peak positions marked as orders of 00*l* reflections.

technique is demonstrated by the complete separation of all the peaks from the different minerals. The strong reflections in the low-angle region particularly are now all in the clear. Let's use everything we have learned at this point (and a little more) to squeeze all the information possible from the diffraction pattern. All five chlorite reflections are now visible, and they allow the following interpretations: (1) the chlorite shows no line broadening pattern caused by interstratification; (2) the nearly equal intensities of the 001 and 003 reflections indicate that the substitution of Fe is symmetrical between the silicate layer and the hydroxide interlayer; and (3) the relative intensities of the five basal chlorite reflections are consistent with a composition of 1.6 Fe atoms per 6 octahedral sites, based on comparisons with calculated diffraction patterns.

Still referring to Fig. 8.14, the dehydrated smectite has its 003 reflection at $d = 3.20 \text{ \AA}$, and that value is consistent with a composition that contains no interstratified chlorite. The value of $d = 9.7 \text{ \AA}$ for the 001 smectite peak might suggest chlorite interstratification, but that shift from the predicted value of 9.6 \AA is also present in the calculated pattern. The shift is caused by the sensitivity of this reflection to particle size effects (Reynolds, 1968; Trunz, 1976). The smectite pattern of the dehydrated sample has fairly strong 001 and 003 peaks, but no detectable 002 reflection, suggesting that it is trioctahedral (or nontronite, a possibility that we will ignore).

Table 8.5 characterizes the corrensite based on the dehydrated preparation (Fig. 8.14). Calculated and observed intensities are in good agreement for a composition of 0.8 Fe atoms per 3 octahedral sites in the chlorite component and 0.8 Fe atoms per 3 octahedral sites in the smectite component. It is interesting that this is the same composition estimated for the chlorite in the sample. The coefficient of variability is 0.29% based on the 002* to the 008* reflections from the dehydrated preparation, indicating almost perfect *R1* ordering with a 50/50 proportion of chlorite to smectite.

We know enough about the minerals to compute a quantitative analysis. The integrated areas were measured for the chlorite 002, the smectite 001, and the corrensite 003* reflections, all from the dehydrated preparation, and using the methods outlined in Chapter 9, we get chlorite 83%, smectite 10%, and corrensite 8% (by weight). Mineral intensity factors were calculated by NEWMOD[©] for chlorite and corrensite using the estimated Fe contents. The intensity ratio of the 002 and 003 reflections from the EG preparation (Fig. 8.14) was matched by a model saponite containing 0.35 Fe per three octahedral sites, and that composition was used in the calculation of the mineral intensity factor for the dehydrated smectite. (See Eq. 9.11 and related discussion for details of this procedure.) Unfortunately, the quantitative analysis presented above is suspect because the sample preparation method used (pipetted glass slide) tends to emphasize the finer particle sizes. It would have been better had we used the filter transfer method described in Chapter 6. In addition, considerable uncertainty lies in the mineral intensity factor for the smectite because it is based on the relative intensities of only two reflections.

Table 8.5. Characterization of corrensite, 0.8 Fe per 3 octahedral sites. Data for the dehydrated preparation (see Fig. 8.14)

Reflection	Integrated intensity (calc.)	Integrated intensity (obs.)
001	2	Not detected
002	125	113
003	173	183
004	26	26
006	19	34
007	115	91

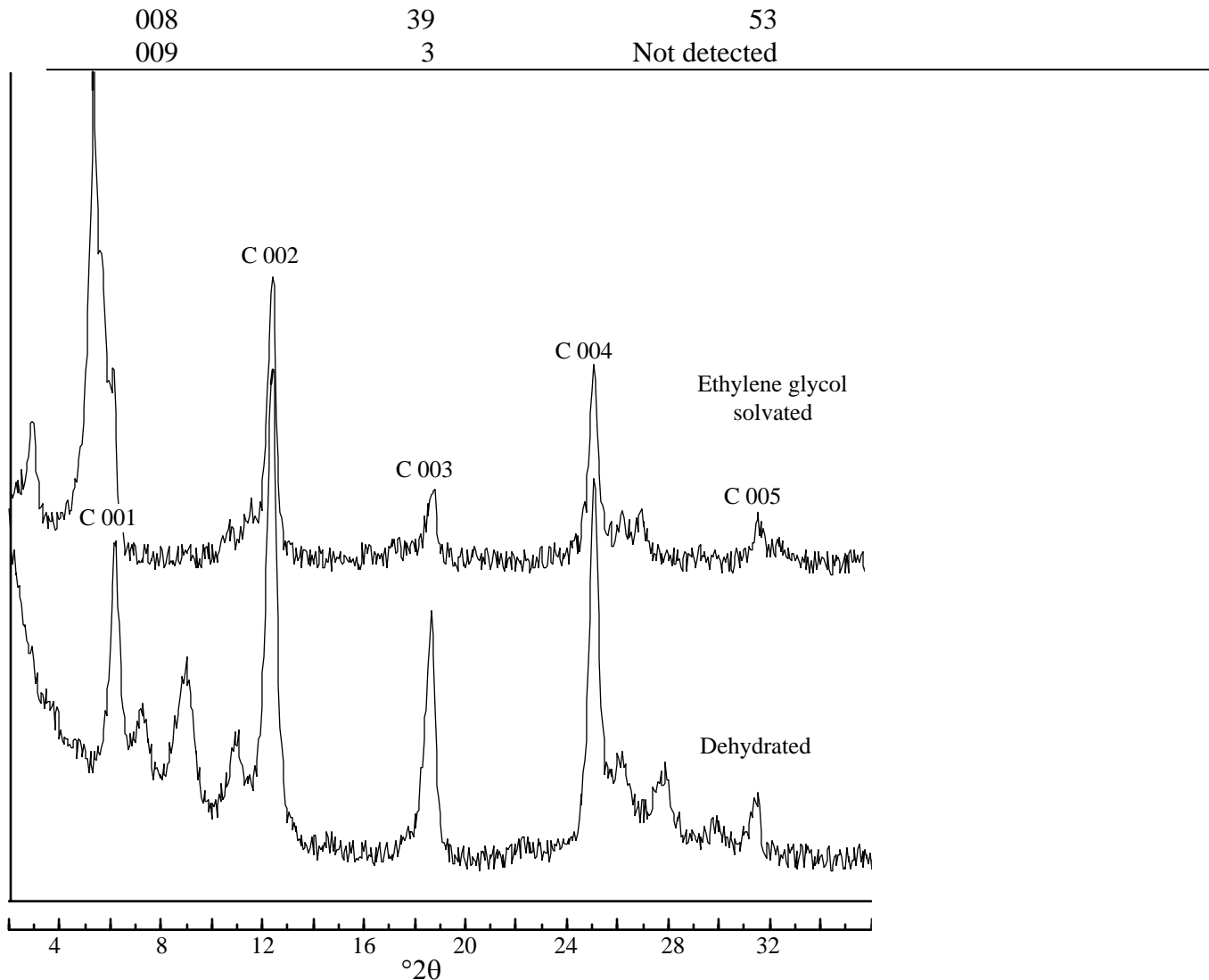


Fig. 8.15. The experimental diffractograms of Fig. 8.14 to which computer-generated noise has been added to simulate poor data.

Figure 8.15 illustrates the experimental diffraction patterns of Fig. 8.14 that have been superimposed on a noisy background to simulate poorer data. Many of the weaker reflections are lost, but you can see that the low-angle region of the dehydrated preparation retains well-resolved diagnostic peaks for the three minerals. A qualitative analysis based on the upper (EG-solvated) trace would inspire less confidence.

Kaolinite/Smectite

The older literature contains few reports of kaolinite/smectite, and all the well-documented occurrences are randomly interstratified (Schultz et al., 1971; Wiewiora, 1971; Sakharov and Drits, 1973; Hughes et al., 1987), except for one example from sandstone that seems to be *R1* kaolinite(0.5)/smectite (Thomas, 1989). However, a recent publication by

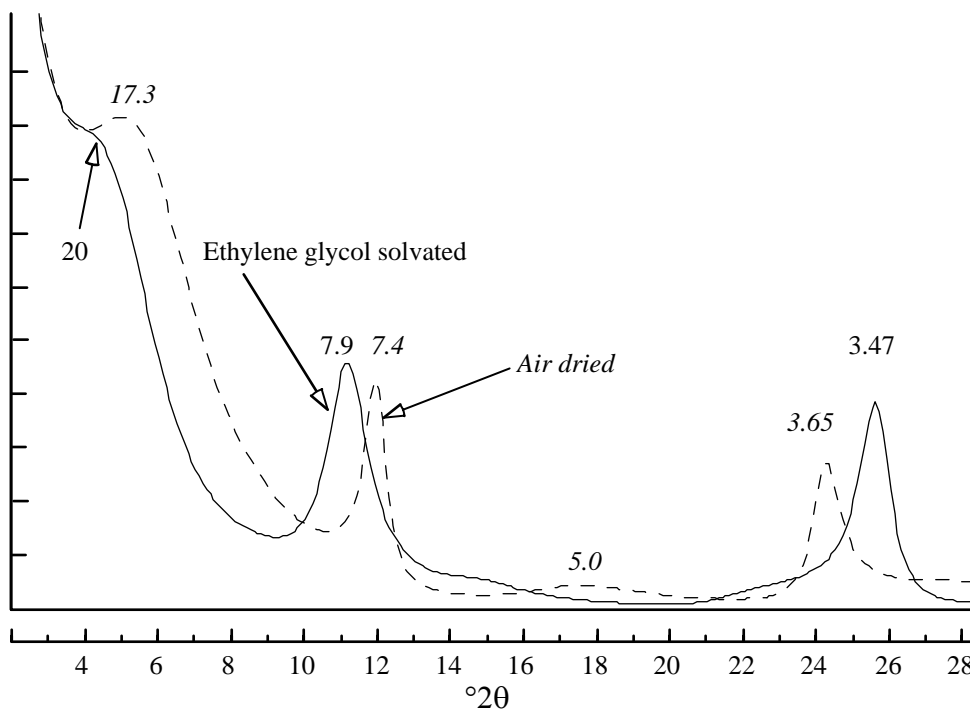


Fig. 8.16. *R0* kaolinite(0.7)/smectite, glycol-solvated and air-dried; peak positions in Ångströms.

Hughes et al. (1993) reports the widespread occurrence of kaolinite/smectite in soils and paleosols ranging in age from Pennsylvanian to Holocene, and they find evidence of *R1* ordering in some of the samples. They suggest that kaolinite-rich kaolinite/smectite may have been overlooked by earlier workers who misidentified some occurrences as either “poorly crystalline” kaolinite or dehydrated halloysite.

Randomly interstratified kaolinite/smectite presents few problems unless it is present as a minor constituent in a clay mixture. Solvation with EG causes easily detected changes in the diffraction pattern with respect to the air-dried preparation (Fig. 8.16). Heat treatments are necessary for definitive interpretations. They change the pattern quite drastically, producing changes that are unintuitive. For the example of *R0* kaolinite(0.7)/smectite (Figs. 8.16, 8.17), the strong reflections at $d = 7.9$ Å (EG solvated) and $d = 7.4$ Å (air dried) increase to 8.1 Å upon heating; so what do we have here—a clay mineral that expands upon heat treatment? No, the reason for the peak displacements is that heating has created 9.7 Å layers ($9^\circ 2\theta$) from 17 and 15 Å layers for the smectite, respectively, and the dehydrated smectite 001 peak has a smaller diffraction angle (larger d) than the 002 reflections from the EG or air-dried preparations. Therefore, the mixed-layered reflection is pulled (i.e., the Méring pull) to a lower angle (larger d) upon collapse of the structure. In case of small amounts of expandable layers, < 10 to 15%, look for a slight smearing of the 17 Å peak in the sense described by Fig. 5.8 and associated text (p. 161).

Figures 8.18 and 8.19 show calculated diffraction patterns for smectite-rich *R0* kaolinite/smectite. Again, the increase in d from 8.3 Å in the EG treated state to 9.4 Å is evident upon heating to 375°C.

The peak positions for EG-solvated kaolinite/smectite produce conventional Méring-type migrations with changing composition, and, as with the other species described above, we recommend the use of the $\Delta 2\theta$ parameter for determining composition. Table 8.6 contains values for the positions of peaks that are useful for determining the composition of randomly interstratified kaolinite/smectite.

The calculated diffraction patterns of Fig. 8.20 give an inkling of why kaolinite/smectite may be under-reported. Suppose that you had run only an air-dried preparation, and further suppose that

equilibration had not occurred between the sample and laboratory humidity, giving a random mixture of one- and two-water-layer smectite interlayers. The trace on Fig. 8.20 labeled “air dried*” is a pattern for kaolinite/smectite with 20% of such mixed expandable layers. Above it, is a pattern for pure kaolinite based on very thin crystallites. Except for the low-angle background, which could be obscured by pure smectite in a real sample, the two patterns have little to distinguish them, and

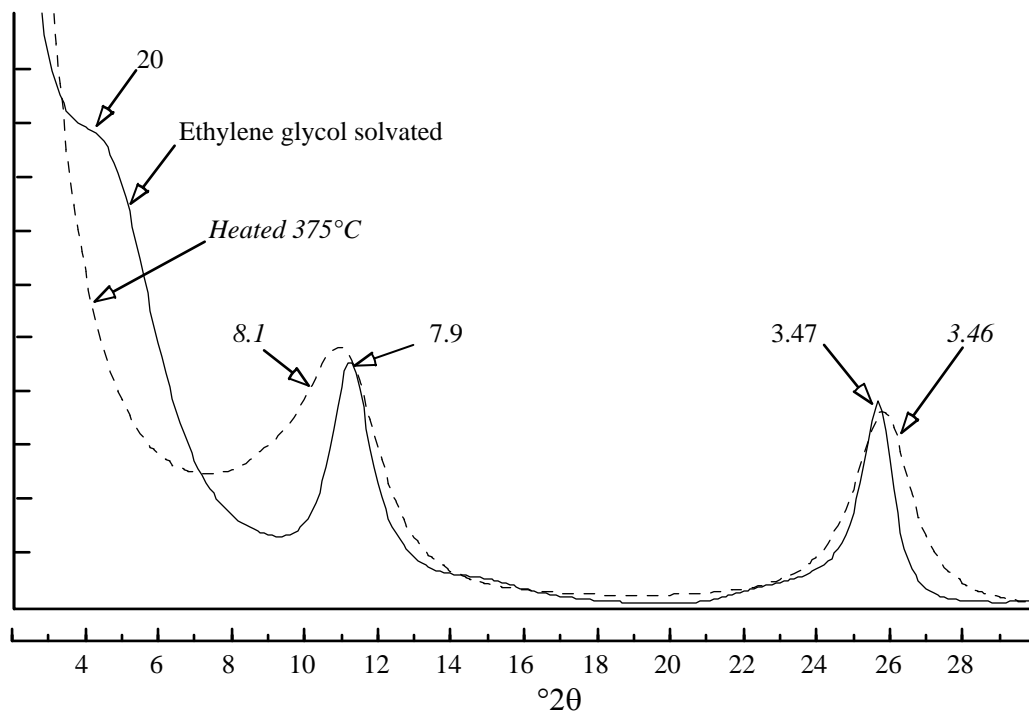


Fig. 8.17. R0 kaolinite(0.7)/smectite, glycol-solvated and heated to 375°C. Peak positions in Ångströms.

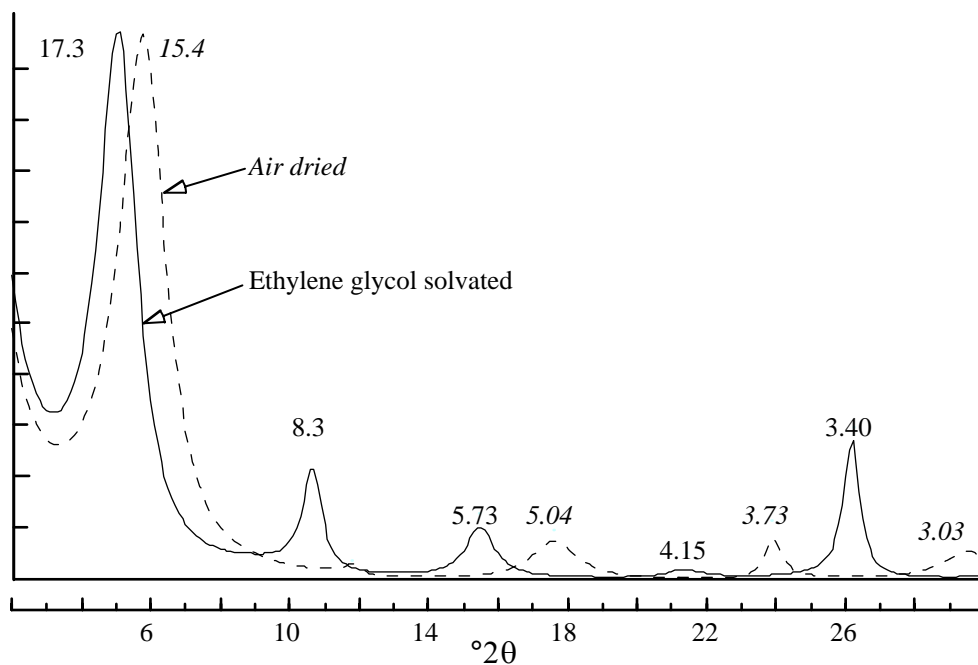


Fig. 8.18. R0 kaolinite(0.3)/smectite, glycol-solvated and air-dried. Peak positions in Ångströms.

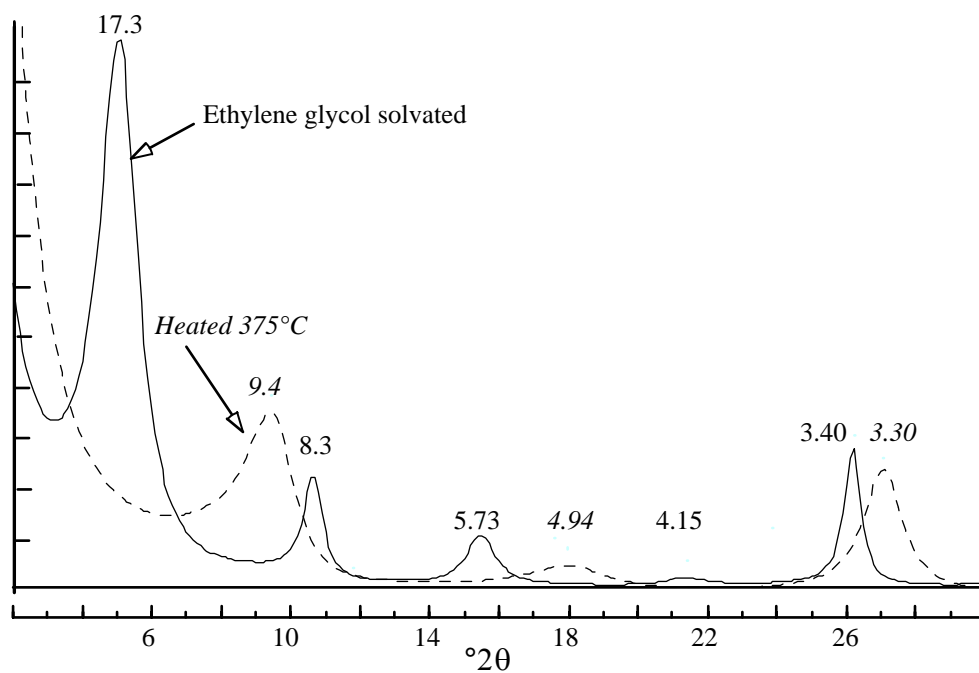


Fig. 8.19. *R0* kaolinite(0.3)/smectite, glycol-solvated and heated to 375°C. Peak positions in Ångströms.

Table 8.6. The positions (CuK α) of useful reflections for estimating percent kaolinite in *R0* kaolinite/EG-smectite

% Kaolinite	001/002		002/005		$\Delta^\circ 2\theta$
	$d(\text{Å})$	$^\circ 2\theta$	$d(\text{Å})$	$^\circ 2\theta$	
10	8.46	10.46	3.39	26.29	15.83
20	8.38	10.56	3.39	26.29	15.73
30	8.31	10.65	3.40	26.21	15.56
40	8.23	10.75	3.41	26.13	15.38
50	8.10	10.92	3.43	25.98	15.06
60	7.98	11.10	3.44	25.90	14.80
70	7.90	11.19	3.47	25.67	14.48
80	7.65	11.57	3.50	25.45	13.88
90	7.43	11.91	3.54	25.16	13.25

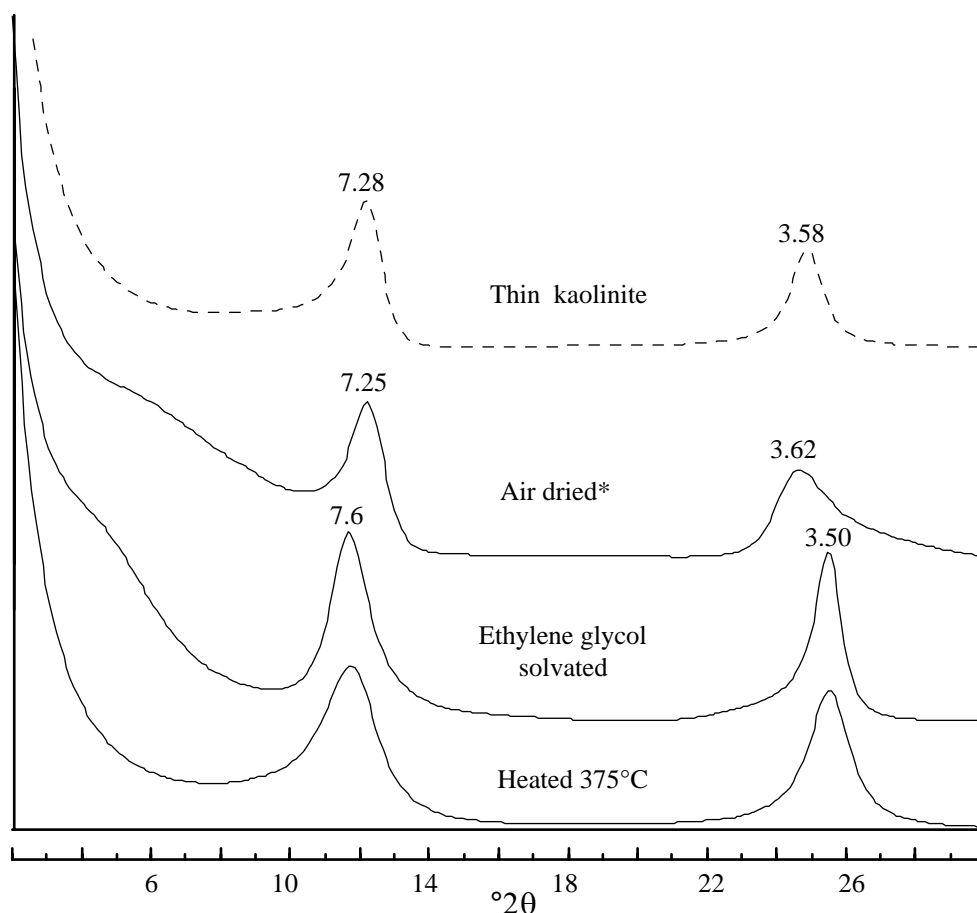


Fig. 8.20. Calculated diffraction patterns for different preparations of *R0* kaolinite(0.8)/smectite compared to pure but finely crystalline kaolinite. The air-dried* simulation depicts a three-component system of randomly interstratified kaolinite (0.8), two-water-layer smectite (0.1) and one-water-layer smectite (0.1). Peak positions in Ångströms.

a diagnosis of kaolinite or dehydrated halloysite (because of the broad reflections) is a reasonable one. Alternatively, you may have data only for heated and EG-solvated states (lower two traces on Fig. 8.20). The mineral contains almost no expandable component because dehydration and EG solvation have only slight to no differential effects—correct? Good thinking, but incorrect in this case. By chance, low-expandability kaolinite/smectite gives almost identical diffraction results for these two structural states. However, assuming that you are unaware of this coincidence, you should be suspicious because the two peaks on the lower traces of Fig. 8.20 are not rationally related. Two times 3.50 Å equals 7.0 Å, and the first peak has a spacing of 7.6 Å. This is an impossible situation, so something must have gone wrong in running the sample. Maybe the goniometer is off. When there is enough time, we will rerun the sample.

The dilemma disappears if all the diffraction data of Fig. 8.20 are considered. There are large changes in *d* between the peaks of the air-dried and the other preparations. These confirm the diagnosis of kaolinite/smectite. Once that is established, go to Table 8.6 and work out the percent of kaolinite in the mixed-layered mineral. We have not shown diffraction patterns for pure one- and two-water-layer structures, but they too show large differences in *d* compared to the EG-solvated and dehydrated cases. This example demonstrates the need for diffraction patterns of all three preparations if kaolinite/smectite is to be confidently identified.

Figures 8.21 and 8.22 show patterns for regularly interstratified (*R1*) kaolinite(0.5)/smectite. This mineral would qualify for a mineral name like corrensitite or rectorite if a specimen could be found that is sufficiently pure to allow complete characterization. Its diffraction characteristics should look like those

of the calculated patterns. Be on the lookout for it, for there is much validity in the idea that you only find what you look for, or as someone has said, I will see it when I believe it.

Serpentine/Chlorite

Recall our discussion of this puzzling mineral in Chapter 5 (pp. 185ff) and our decision to call it serpentine/chlorite. However, the calculated X-ray diffraction patterns of serpentine/chlorite and kaolinite/chlorite are indistinguishable at the low concentrations of 7 Å layers so far reported for this mineral. The structures of 7 Å/chlorite mixed-layered clay minerals have unique characteristics that place them in their own diffraction class. The basal spacing of chlorite is very nearly twice that of the 7 Å component, so that reflections from the 7 Å component fall almost exactly on all even-order chlorite peaks. This structure provides the paradoxical situation of a randomly interstratified mineral that produces a rational 00 l diffraction pattern whose peak positions are independent of composition.

Because the 1:1 layer is ~7 Å and chlorite is ~14 Å, when they are interstratified, X-ray diffraction tracings of the odd-numbered 00 l peaks are

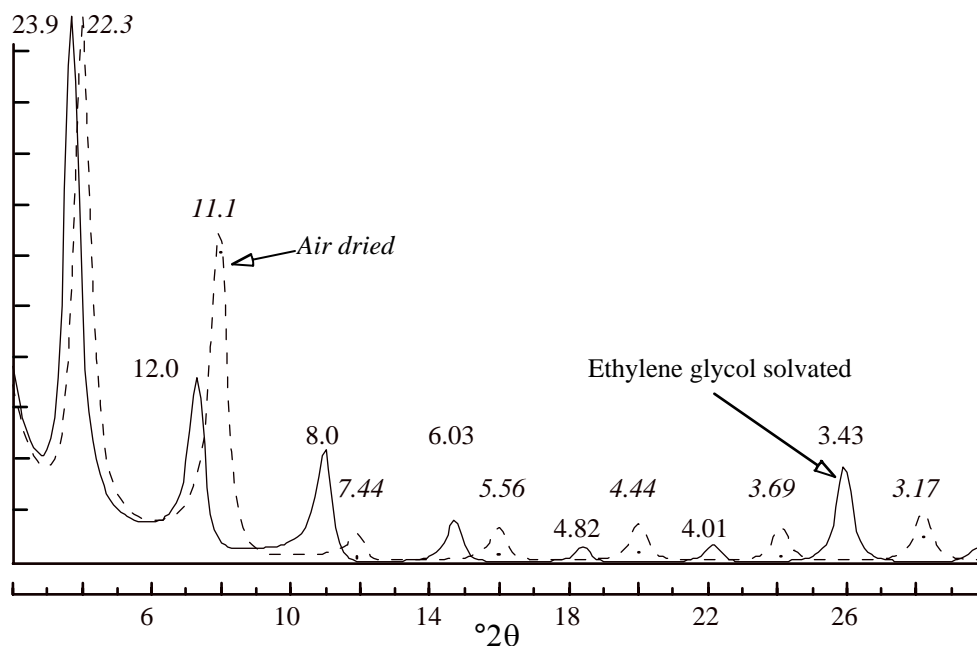


Fig. 8.21. R1 kaolinite(0.5)/smectite, glycol-solvated and air-dried. Peak positions in Ångströms.

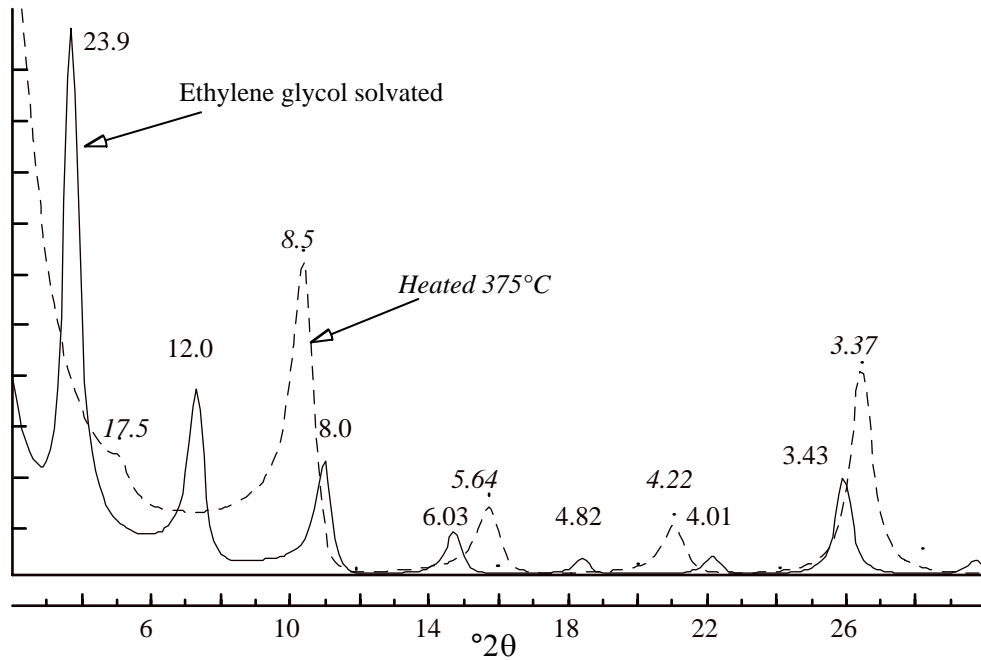


Fig. 8.22. R1 kaolinite(0.5)/smectite, glycol-solvated and heated to 375°C. Peak positions in Ångströms.

broadened. Can you see why? Recall that the 001 peak of chlorite represents diffraction from a 14 Å spacing and that the 002 peak represents the 14 Å spacing behaving as if it were a 7 Å spacing, i.e., the n of $n\lambda = 2d\sin\theta$ is one for the 001 peak and two for the 002 peak. Can you see from this that all even-numbered reflections will behave like 7 Å/ n spacings, and that the 7 Å 1:1 layers diffract constructively with these even-ordered reflections from the 14 Å layers? (It may help to return to Chapter 3, where Fig. 3.13 is discussed on pp. 85ff.) In the case of what would otherwise be the chlorite $d(001)/1$, the interstratified 7 Å 1:1 layers break up the stack of 14 Å layers by acting as defects, but the 7 Å spacing of the 1:1 layers matches the repeat distance along the Z^* for the reflection from the $d(001)/2$ spacing. So, effectively, N is relatively small for the odd-numbered peaks, and they, therefore, have broad peaks. And N is large for the even-numbered ones and will have relatively sharp peaks (Reynolds et al., 1992). Do we need to remind you of the Scherrer equation (Eq. 3.8)?

We also can use Méring's principles in order to explain the character of the diffraction pattern. Remember, peaks are broad if end-member reflections are widely separated. Conversely, sharp peaks indicate the close juxtaposition of reflections from both components. For serpentine/chlorite, all odd-order chlorite peaks are well separated from any serpentine reflection, and chlorite even-order reflections are virtually superimposed on the serpentine peak positions (Fig. 8.23).

Reynolds et al. (1992) discussed in detail the X-ray diffraction characteristics of one specimen of serpentine/chlorite from the Tuscaloosa sandstone of the Gulf Coast region, and developed an empirical formula for estimating the percent serpentine present (Eqs. 8.1 and 8.2). Its application requires that the diffractograms be obtained using two Soller slits (2°), a 1° beam slit, and a 0.05° detector slit. Finer slits can be used but are unnecessary. Reynolds et al. recommend using the 004 and 005 chlorite reflections.

$$\beta_r = \left(\beta_{005}^{1.25} - \beta_{004}^{1.25} \right)^{\frac{1}{1.25}} \quad (8.1)$$

and

$$\% \text{ Serpentine} = -0.51 + 24.27\beta_r \quad (8.2)$$

The quantity β_r in Eqs. (8.1 and 8.2) denotes the breadth of the 005 reflection, corrected for the baseline breadth of the 004, which contains no mixed-layered broadening. You might look at Eq. (8.2) and think, this can't be correct. What if there is no mixed-layering? Then β_r is zero, and if I substitute zero into Eq. (8.2), the result is -0.51% serpentine. Your reasoning is correct. But remember that these equations are empirical, or in other words,

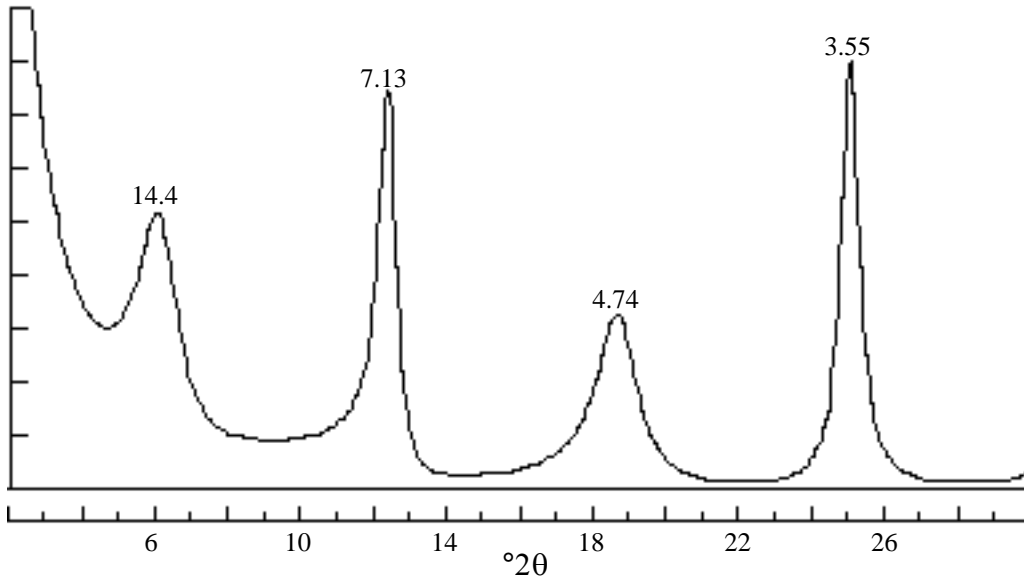


Fig. 8.23. Trioctahedral *R0* serpentine(0.2)/chlorite, Mg end-members. Peak positions in Ångströms.

they are not based on first principles. Clearly, they cannot apply to very low proportions of serpentine. In fact, they apply very well only to the range of 1-20% serpentine (*R0*), which is the likely range for natural occurrences of this mixed-layered mineral. Your measurement of line breadth is not going to be accurate enough anyway to allow you to deal with compositions that have less than 1% serpentine.

In summary, serpentine/chlorite or kaolinite/chlorite have peaks with rational positions that are fixed despite the proportions of end-members, but increasing percentages of interstratified serpentine or kaolinite cause increased broadening of odd-order chlorite reflections with respect to even orders (Fig. 8.23). The minerals are unaffected by liquid solvation and/or moderate heat treatments.

Mica/Vermiculite

Mixed-layered trioctahedral mica/vermiculite is uncommon in sedimentary rocks, but it is widespread in hydrothermal and soil clay mineral suites. The regularly interstratified phase, containing 50% mica, was one of the first ordered interstratified clay minerals to be recognized. It was described by Gruner (1934) who called it hydrobiotite. Its calculated diffraction pattern is shown in Fig. 8.24. The regular Bragg series of spacings results from a $d(001)^*$ of 24.4 Å in the air-dried state. Collapse of the vermiculite component by heat treatment produces a rational pattern that looks like that of a simple mica with $d(001) = 10$ Å. In fact, the dehydrated vermiculite spacing may be a bit more than 10 Å because heat-treated vermiculites rarely collapse

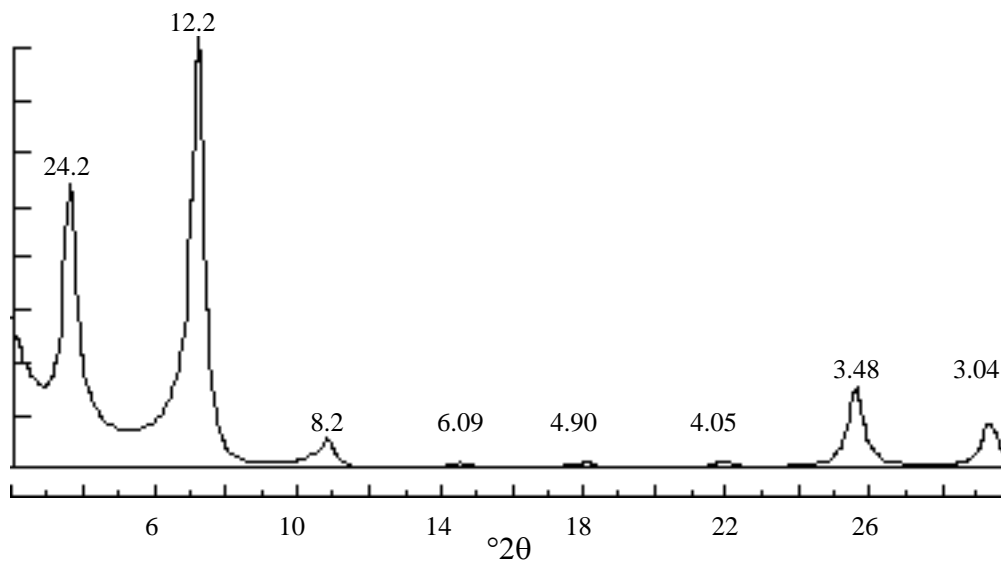


Fig. 8.24. Hydrobiotite (trioctahedral) air-dried [*R1* biotite(0.5)/vermiculite]. Silicate octahedral sheets contain 1 Fe per 3 sites. Peak positions in Ångströms.

that much; a value of 10.3 Å for the apparent 001 reflection squares better with experience, so $d(001)$ may be closer to 10.15 Å. The collapsed phase produces a very weak reflection near $d = 5$ Å because of heavy out-of-phase (with respect to the rest of the silicate skeleton) octahedral scattering caused by the trioctahedral character and augmented by the likelihood of significant amounts of Fe in those sites. Its diffraction pattern resembles that of glauconite. Proof of a vermiculite component requires that you saturate with Mg, completely solvate with glycerol, and obtain a diffraction pattern that is essentially unchanged from that of the air-dried condition.

Figure 8.25 shows the diffraction pattern for trioctahedral *R1* mica(0.65)/vermiculite. You can see the similarities to the hydrobiotite pattern in this diffractogram, but, as you would expect, peaks have shifted as a result of the increased mica content and the randomness that is present because the composition is not 50/50. The superstructure reflection (001*) is reduced to a low shoulder on the low-angle background. Estimates of composition for these minerals are usually based on the position of the 001/ 002* reflection because, for most samples, that is the only one you are likely to see. Table 8.7 shows the position of this reflection as a function of composition together with peak positions for the *R0* mica/vermiculite 001/002 and 003/004 reflections.

Figures 8.26 and 8.27 give examples of randomly and *R1* ordered, interstratified trioctahedral mica/vermiculite. The patterns for *R0* are simpler than those for *R1* because there are no superstructure components in the reflections. The low-angle reflection (001/001) is usually the most practical to use for estimates of composition (Table 8.7).

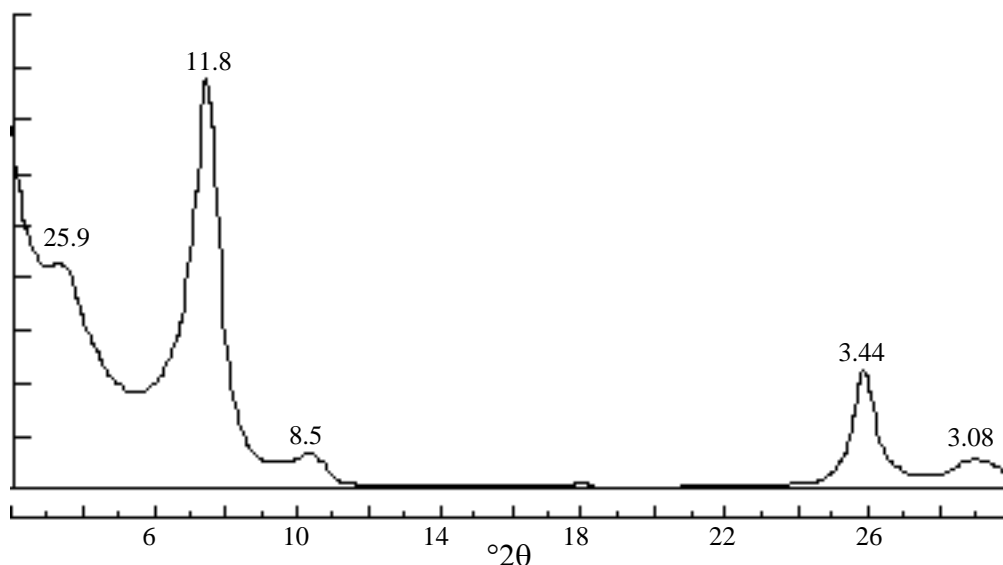


Fig. 8.25. Trioctahedral *R1* mica(0.65)/vermiculite. Silicate octahedral sheets contain 1 Fe per 3 sites. Peak positions in Ångströms.

Identifying *R0* versus *R1* ordering is difficult if the mica content is greater than about 80%. Figure 8.27 shows a pattern for 80% mica, *R1*. Its identity is indicated by the subtle high-angle shoulder on the 001/001 reflection. This shoulder is the 001/003*, and it is more obvious at compositions that contain less than 70% mica (see Fig. 8.25). (Here is a good example of how subtle features of peak shape can be important.)

We will not discuss the diffraction characteristics of dioctahedral chlorite/smectite and dioctahedral illite/vermiculite because the basal diffraction patterns for these resemble those of the trioctahedral varieties.

Table 8.7. The positions (CuK α) of useful reflections for estimating percent vermiculite in trioctahedral mica/vermiculite (air dried)

% Vermiculite	<i>R0</i>		<i>R1</i>	
	$d(\text{Å})$	$^{\circ} 2\theta$	$d(\text{Å})$	$^{\circ} 2\theta$
10	10.27	8.61	3.35	26.61
20	10.90	8.11	3.38	26.37
40	12.53	7.05	3.45	25.82
50	13.02	6.79	3.48	25.60
60	13.43	6.58	3.51	25.37
70	13.75	6.43	3.53	25.23
80	13.97	6.33	3.55	25.08
90	14.17	6.24	3.57	24.94

*Indicates that the 002 is a basal spacing for a superstructure.

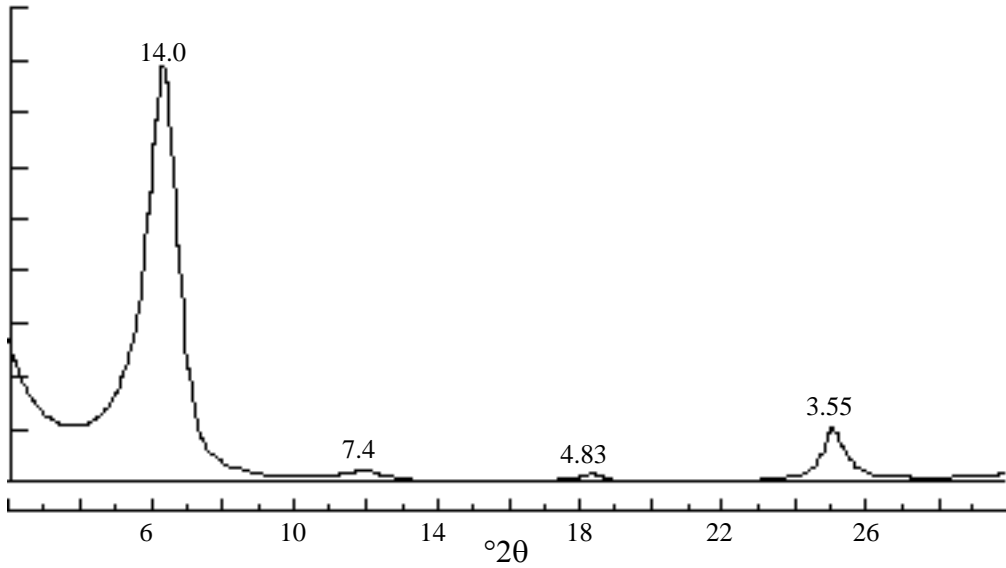


Fig. 8.26. Trioctahedral *R1* mica(0.2)/vermiculite. Silicate octahedral sheets contain 1 Fe per 3 sites. Peak positions in Ångströms.

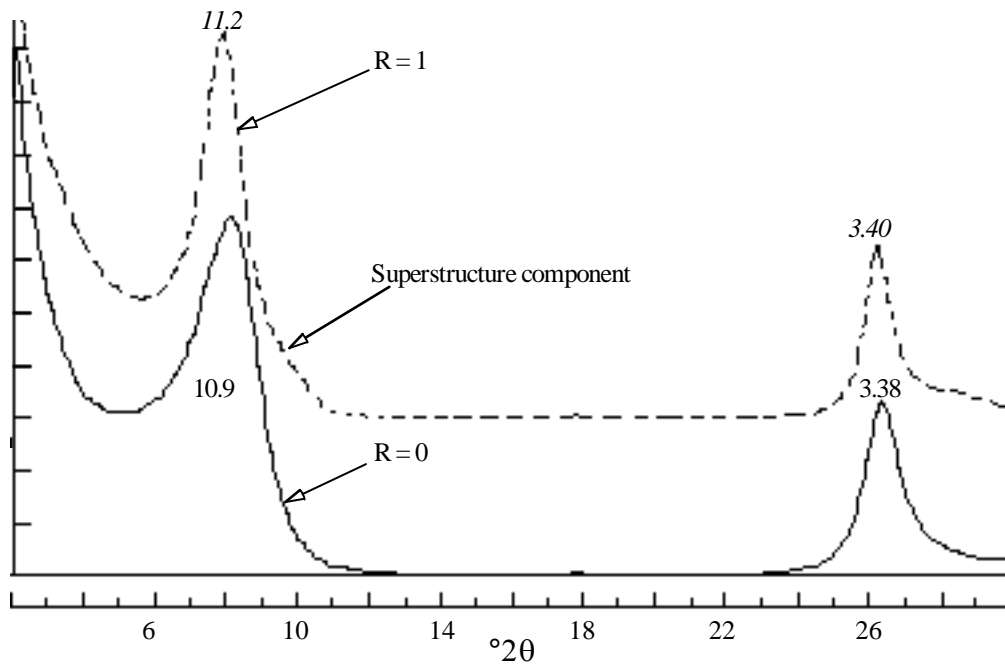


Fig. 8.27. *R1* and *R0* trioctahedral mica(0.8)/vermiculite. Silicate octahedral sheets contain 1 Fe per 3 sites. Peak positions in Ångströms.

Peak intensities differ, but peak position is not much affected by the composition of the octahedral layers. The identification of dioctahedral types is best based on the position of the 060 reflection (Chapter 7).

SUMMARY

Identifying clay minerals from their diffraction tracings is something of a *Gestalt* process, i.e., identifying the whole—being able to say that it is an illite/smectite because it has an illite/smectite pattern. The mixed-layered clay minerals with any appreciable degree of randomness to their interstratification show an irrational series of peaks. Relative broadness of peaks on a single pattern varies for these clay minerals, unlike peaks for discrete clay minerals or nonclay minerals. And the peaks of mixed-layered clay minerals can be much broader than those of discrete clay minerals. Mixed-layered line broadening is a function of the separation of the peaks of the two components that are incorporated into one peak (Fig. 8.1). The most useful tool for identifying mixed-layered clay minerals is the modeling of their 00 l diffraction tracings for comparison to experimental diffractograms.

REFERENCES

- Bailey, S. W. (1982) Nomenclature for regular interstratifications: *Amer. Minerl.* **67**, 394-98.
- Brindley, G. W., and Gillery, F. H. (1953) A mixed-layer kaolin-chlorite structure: in Swineford, A., and Plummer, N., editors, *Proceedings, 2nd National Conf. on Clays and Clay Minerals*, Columbia, Missouri, Pub. 327, Natl. Academy of Sciences-Natl. Research Council, 349-53.
- Gruner, J. W. (1934) The structure of vermiculites and their collapse by dehydration: *Amer. Minerl.* **19**, 557-78.
- Hillier, S. (1995) Mafic phyllosilicates in low grade metabasites: Characterization using deconvolution analysis discussion: *Clay Minerals* **30**, 67-73.
- Hughes, R. E., DeMaris, P. J., White, W. A., and Cowin, D. K. (1987) Origin of clay minerals in Pennsylvanian strata of the Illinois Basin: in Schultz, L. G., van Olphen, H., and Mumpton, F. A., editors, *Proceedings, Internatl. Clay Conf.*, Denver, 1985, The Clay Minerals Society, Bloomington, Indiana., 97-104.
- Hughes, R. E., Moore, D. M., and Reynolds, R. C., Jr., (1993) The nature, detection, occurrence, and origin of kaolinite/smectite: in Murray, H., Bundy, W., and Harvey, C., editors, *Kaolin: Genesis and Utilization*, Special Pub. No. 1, The Clay Minerals Society, 291-323.
- Klug, H. A., and Alexander, L. E. (1974) *X-Ray Diffraction Procedures*: J. Wiley, New York, 966 pp.
- Lippmann, F. (1956) Clay minerals from the Roet member of the Triassic near Goettingen, Germany: *J. Sed. Pet.* **26**, 125-39.
- MacEwan, D. M. C. (1958) Fourier transform methods for studying X-ray scattering from lamellar systems. II. The calculation of X-ray diffraction effects for various types of interstratification: *Kolloidzeitschrift* **156**, 61-7.
- Méring, J. (1949) L'Intéférence des Rayons X dans les systèmes à stratification dé sordonnée: *Acta Crystallogr.* **2**, 371-77.
- Reynolds, R. C., Jr. (1967) Interstratified clay systems: calculation of the total one-dimensional diffraction function: *Amer. Minerl.* **52**, 661-73.
- Reynolds, R. C., Jr. (1968) The effect of particle size on apparent lattice spacings: *Acta Crystallogr.* **A24**, pt. 2, 319-20.
- Reynolds, R. C., Jr. (1980) Interstratified clay minerals: in Brindley, G. W., and Brown, G., editors, *Crystal Structures of Clay Minerals and Their X-Ray Identification*: Monograph No. 5, Mineralogical Society, London, 249-303.
- Reynolds, R. C., Jr., and Hower, J. (1970) The nature of interlayering in mixed-layer illite-montmorillonite: *Clays and Clay Minerals* **18**, 25-36.
- Reynolds, R. C., Jr. (1985) *NEWMOD, A Computer Program for the Calculation of the Basal Diffraction Intensities of Mixed-Layered Clay Minerals*: R. C. Reynolds, 8 Brook Rd. Hanover NH.
- Reynolds, R. C., Jr., Distefano, M. P., and Lahann, R. W. (1992) Randomly interstratified serpentine/chlorite: Its detection and quantification by powder X-ray diffraction methods: *Clays and Clay Minerals* **40**, 262-67.
- Robinson, D., and Bevins, R. E. (1994) Mafic phyllosilicates in low grade metabasites: Characterization using deconvolution analysis: *Clay Minerals* **29**, 223-37.
- Sakharov, B. A., and Drits, V. A. (1973) Mixed-layer kaolinite-montmorillonite. A comparison of observed and calculated diffraction patterns: *Clays and Clay Minerals* **21**, 15-17.
- Schultz, L. G., Shepard, A. O., Blackmon, P. D., and Starkey, H. C. (1971) Mixed-layer kaolinite-montmorillonite from the Yucatan Peninsula, Mexico: *Clays and Clay Minerals* **19**, 137-50.
- Š rodoň , J. (1980) Precise identification of illite/smectite interstratifications by X-ray powder diffraction: *Clays and Clay Minerals* **28**, 401-11.
- Thomas, A. R. (1989) A new mixed layer mineral—Regular 1:1 mixed layer kaolinite/smectite: *Programs with Abstracts: 26th Annual Meeting The Clay Minerals Society*, Sacramento, California, 69.
- Trunz, V. (1976) The influence of crystallite size on the apparent basal spacings of kaolinite: *Clays and Clay Minerals* **24**, 84-7.
- Vivaldi, J. L. M., and MacEwan, D. M. C. (1957) Triassic chlorites from the Jura and Catalan Coastal Range: *Clay Min. Bull.* **3**, 177-83.
- Walker, G. F. (1957) On the differentiation of vermiculites and smectites in clays: *Clay Min. Bull.* **3**, 154-63.
- Wiewiora, A. (1971) A mixed-layer kaolinite-smectite from Lower Silesia, Poland: *Clays and Clay Minerals* **19**, 415-16.